

# Unexpected high abyssal ophiuroid diversity in polymetallic nodule fields of the Northeast Pacific Ocean, and implications for conservation

Magdalini Christodoulou<sup>1</sup>, Timothy O'Hara<sup>2</sup>, Andrew Hugall<sup>2</sup>, Sahar Khodami<sup>1</sup>, Clara F. Rodrigues<sup>3</sup>, Ana Hilario<sup>3</sup>, Annemiek Vink<sup>4</sup>, Pedro Martinez Arbizu<sup>1</sup>

<sup>1</sup>German Centre for Marine Biodiversity Research (DZMB), Senckenberg am Meer, Wilhelmshaven, 26382, Germany

<sup>2</sup>Laboratory example, city, postal code, country Museums Victoria, Melbourne, 3001, Australia

<sup>3</sup>Centre for Environmental and Marine Studies (CESAM), Department of Biology, University of Aveiro, Aveiro, 3810-193, Portugal

10 <sup>4</sup>Federal Institute for Geosciences and Natural Resources, Marine Geology, 30655, Hannover, Germany

*Correspondence to:* Magdalini Christodoulou (magdalini.christodoulou@senckenberg.de)

**Abstract.** The largest and commercially appealing mineral deposits can be found in the abyssal seafloor of the Clarion-Clipperton Zone (CCZ), a polymetallic nodule province, in the NE Pacific Ocean, where experimental mining is due to take  
15 place. In anticipation of deep-sea mining impacts, it has become essential to rapidly and accurately assess biodiversity. For this reason, ophiuroid material collected during eight scientific cruises from five exploration license areas within CCZ, one area protected from mining (APEI3, Area of Particular Environmental Interest) in the periphery of CCZ and the DIS-turbance and re-COLonisation (DISCOL) Experimental Area (DEA), in the SE Pacific Ocean, was examined. Specimens were genetically analysed using a fragment of the mitochondrial cytochrome c oxidase subunit I (COI). Maximum Likelihood and  
20 Neighbour Joining trees were constructed, while four tree-based and distance-based methods of species delineation (ABGD, BINs, GMYC, mPTP) were employed to propose Secondary Species Hypotheses (SSHs) within the ophiuroids collected. The species delimitations analyses concordant results revealed the presence of 43 deep-sea brittle stars SSHs, revealing an unexpectedly high diversity and showing that the most conspicuous invertebrates in abyssal plains have been so far considerably under-estimated. The number of SSHs found in each area varied from 5 (IFREMER area) to 24 (BGR area),  
25 while 13 SSHs were represented by singletons. None of the SSHs was found to be present in all 7 areas, while the majority of species (44.2 %) had a single-area presence (19 SSHs). The most common species were Ophioleucidae sp. (Species 29), *Amphioplus daleus* (Species 2) and *Ophiosphalma glabrum* (Species 3), present in all areas except APEI3. The biodiversity patterns could be mainly attributed to POC fluxes that could explain the highest species numbers found in BGR (German contractor area) and UKSRL (UK contractor area) areas. The five exploration contract areas belong to a mesotrophic province,  
30 while in contrary the APEI3 is located in an oligotrophic province which could explain the lowest diversity as well as very low similarity with the other six study areas. Based on these results the representativeness and the appropriateness of APEI3 to meet its purpose of preserving the biodiversity of the CCZ fauna are questioned. Finally, this study provides the foundation

for biogeographic and functional analyses that will provide insight into the drivers of species diversity and its role in ecosystem function.

## 35 **1 Introduction**

The deep sea holds the vastest and least explored ecosystems on Earth, and has justifiably being characterised as the “Earth’s Last Frontier” since research and exploration in these areas is still incomplete at the very best (Ramirez-Llodra et al., 2010; Danovaro et al., 2017). Deep-sea habitats cover more than 65% of the Earth’s surface and can plunge from water depths of 200 m (below the continental shelf) to as deep as 11 kilometres in the Mariana Trench (Gage and Tyler, 1991; Carney, 2005; 40 Jamieson et al., 2009; Ramirez-Llodra, et al., 2011). Abyssal ecosystems, found between 3000 m and 6000 m, cover 54% of the Earth’s surface and constitute a network of plains and arising hills and seamounts, segmented by mid-ocean ridges, island arcs and ocean trenches (Gage and Tyler, 1991; Carney, 2005; Smith et al., 2008). The abyssal plains represent perhaps the single largest contiguous ecosystem of our planet, nevertheless because of its enormous size and seclusion it has been the least studied (Smith et al., 2008; Ramirez-Llodra et al., 2010). The seafloor of the abyssal plains is mostly covered by fine sediments, 45 while hard substrates often occur in the form of polymetallic nodules (Smith et al., 2008; Ramirez-Llodra et al., 2011).

Metal-rich (polymetallic) nodules from the deep-sea floor were described and their potential economic importance acknowledged as early as 1873, during the HMS Challenger expedition (Murray and Renard, 1891; Lusty and Murton, 2018). However, it was in the 1960s that economic interest in these deposits was ignited after polymetallic nodule resources in the Pacific Ocean were estimated to be so abundant, as to be an essentially endless supply of metals such as Mn, Cu, Ni, and Co 50 (Mero, 1965; Lusty and Murton, 2018). Despite the optimism in the 1970s and 1980s and the widely held belief that deep-sea mining would commence before the end of 2000, subsequent progress has been slow and unsteady. The adequate supply of metals from land-based mines, unfavourable economic conditions (e.g. rising energy costs, lower metal prices), technological challenges, increasing environmental awareness, and legal obligations to international organisations (e.g. lack of a mining legislation for the deep-sea) were some of the reasons slowing down deep-sea mining (Lusty and Murton, 2018). However, 55 the growing global demand for these metals coupled with the increasing challenges of land-based mining (Calas, 2017), and the advances in mining technology, drove a renewed interest in the exploitation of deep-sea mineral deposits (Ramirez-Llodra et al., 2011; Lusty and Murton, 2018; Miller et al., 2018).

The greatest known accumulations of economically interesting Ni and Cu, Co-rich polymetallic (Fe–Mn) nodules occur in the Clarion-Clipperton Zone (CCZ), extending over an area of approximately 6 million km<sup>2</sup> in size, between Hawaii and Mexico 60 from 120°W to approximately 160°W and from 20°N to 6°S. Additional, important, occurrences have been found in the Central Indian Ocean Basin, the Cook Islands area and the Peru Basin off South America (e.g. the DISCOL Experimental Area, DEA) (Mukhopadhyay et al., 2008; Hein et al., 2013; Miller et al., 2018). The CCZ lies in Areas beyond National Jurisdiction, and thus falls under the legal mandate of the International Seabed Authority, ISA (Wedding et al., 2013). So far, sixteen license areas for the exploration of polymetallic nodules have been approved by the ISA within the CCZ, each up to 75,000 km<sup>2</sup> in

65 size (Wedding et al., 2013). In its environmental management plan for the CCZ (Lodge et al., 2014), the ISA adopted nine  
large protection areas defined as Areas of Particular Environmental Interest (APEI), where mining will not be permitted (Lodge  
et al., 2014). These APEIs are large enough (each of them 400 x 400 km) and far enough away apart from potential mining  
areas that they will not be affected by deep-sea mining (Wedding et al., 2013). In order to be effective as source populations  
70 for the recolonization of impacted areas, however, APEIs should harbour a representative subset of the fauna found in the  
potential fields. In addition to these protection measures, the ISA has stipulated that prior to exploitation, a benthic biological  
baseline study must be undertaken for each exploration contract area, and the possible environmental impacts arising from  
exploration should be assessed. Nodule mining carries significant environmental concerns, including negative direct and  
indirect impacts on the biodiversity (Ramirez-Llodra et al., 2011; Vanreusel et al., 2016; Van Dover et al., 2017; Niner et al.,  
2018). The removal of the nodules and associated organisms could result in habitat loss, fragmentation, or modification, while  
75 the generation of sediment plumes may bury the organisms or clog their feeding apparatuses and thus disrupting the food-webs  
(Ramirez-Llodra et al., 2011; Vanreusel et al., 2016; Van Dover et al., 2017; Niner et al., 2018; Stratmann et al., 2018).  
Unfortunately, accurate documentation of species diversity, which comprises the first step in understanding patterns and  
structures in different levels of biodiversity, biogeographical and ecological processes and is essential for marine ecosystems'  
management, remains poor across the CCZ (Amon et al., 2016). To date, Taboada et al. (2018), although dealing with a single  
80 hexactinellid sponge species, is the only study that has assessed the effectiveness of an APEI (#6) or investigated connectivity  
with the adjacent potential mining areas. Thus, prior to exploitation, there is an urgent need to obtain baseline data on faunal  
biodiversity at local and regional scales in order to assess and predict the effects of mining on deep-sea organisms.

The Ophiuroidea (brittle stars and basket stars) are amongst the most emblematic mobile megafaunal inhabitants of the deep  
sea regarding species diversity and individuals' numbers (Gage and Tyler, 1991; Rex and Etter, 2010; Vanreusel et al., 2016).  
85 They constitute the most diverse echinoderm class, numbering more than 2064 species found in all oceans, from intertidal to  
hadal depths (Stöhr et al., 2012; Jamieson, 2015). Since then, at least 1412 species have been recorded from the deep sea of  
which only 109 are from abyssal depths, despite abyssal plains being the most extensive ecosystem in the world (Stöhr et al.,  
2012). Studies describing the tropical abyssal Northeast Pacific ophiuroid fauna are scarce, including few historical studies  
resulting from the great expeditions of the late nineteenth and early twentieth centuries such as the HMS Challenger (Lyman,  
90 1878, 1879, 1882; Ludwig, 1898, 1899) and the Albatross (Clark, 1911; Clark, 1949). Limited recent studies exist (Amon et  
al., 2016, 2017; Glover et al., 2016), reporting only a small number of species. Consequently, the diversity of the deep-sea  
ophiuroid fauna in the CCZ is only poorly known. Thus the main objectives of this study were to: 1) ensure the future molecular  
species identification for all different life-cycle stages by matching morphology-based species identifications of adult  
ophiuroids with molecular species assignments using COI sequences and consequently compiling a comprehensive reference  
95 library; 2) determine species ranges; 3) describe the ophiuroid biodiversity patterns of the CCZ and the DEA; 4) explore the  
usefulness of APEI3 for the preservation of the ophiuroid nodule fauna in the CCZ in the case of deep-sea mining.

## 2 Material and Methods

### 2.1 Study areas

The study areas are located within the Clarion and Clipperton Fracture Zone (CCZ) in the northeast equatorial Pacific Ocean and at the DISCOL Experimental Area (DEA) in the Peru Basin (Fig. 1), at depths varying from 4050 m to 4933 m (Hein et al., 2013). The CCZ is characterized by gradual changes of environmental conditions (e.g. differences in surface-water productivity, depth and sediment characteristics) across an east-west and a north-south axis, that corresponds to a variation in nodule size and coverage, as well as variations in faunal composition along these gradients (Wedding et al., 2013). Ophiuroid samples were collected from CCZ during six scientific cruises from five different exploration licence areas and one area protected from mining (APEI3). Specifically ophiuroid samples were collected during the following cruises: BioNod on R/V *L'Atalante* (29th March–10th May 2012) to the eastern IFREMER (Institut Français de Recherche pour l'Exploitation de la Mer, France) License Area and to the eastern BGR (Federal Institute for Geosciences and Natural Resources, Germany) Licence Area; two ABYSSLINE research cruises, AB01 on the R/V *Melville* (October 3rd–27th 2013), and the AB02 cruise on the R/V *Thompson* (February 12th–25th March 2015) to the UKSRL License Area (UK Seabed Resources Ltd, United Kingdom); two MANGAN cruises, MANGAN 2013 on R/V *Kilo Moana* (1st April–13th May 2013), and MANGAN 2014 on R/V *Kilo Moana* (15th April–3rd June 2014) to the eastern BGR Area; the scientific cruise EcoResponse on R/V *Sonne* (SO239) (11th March–30th April 2015) to the Licence Areas of BGR, GSR (G-TEC Sea Mineral Resources NV, Belgium), IOM (Interoceanmetal Joint Organization, a country consortium of Bulgaria, Cuba, Czech Republic, Poland, Russian Federation, and Slovakia), IFREMER and APEI3. Furthermore, the area Discol Experimental Area (DEA) in the Peru Basin, in which the German project DISCOL (DISturbance and reCOLonisation experiment) was performed in the late 1980ies (Thiel and Schriever, 1990; Thiel et al., 2001), was recently revisited in the framework of the JPIO Pilot Action “Ecological Aspects of Deep-Sea Mining”. Ophiuroid samples were collected from the DEA during two cruises, SO242/1 and SO242/2 on the R/V *Sonne* from 28th July to 25th August 2015 and 28th August to 1st October 2015 respectively.

### 2.2 Specimen sampling and processing

Small-sized ophiuroid samples were collected using a Brenke-type epibenthic sledge (EBS; Brenke, 2005) from the UKSRL (5 deployments), BGR (15 deployments), IFREMER (4 deployments), GSR (4 deployments), and IOM (1 deployment) license areas, the APEI3 (3 deployments) and the DEA (9 deployments) (Fig. 1), following standard deployment procedures (Brenke, 2005). The cod ends of the supra- and epi-net were sieved through a 500 µm- and 300 µm-mesh with cold (+10°C) sea water and immediately transferred to pre-cooled (-20°C) 96% EtOH. Large-sized ophiuroid samples were collected with a remotely operated vehicle (ROV Kiel 6000, GEOMAR) using either the ROV's suction sampler or the ROV's manipulator arm by direct picking, manipulating scoops, shovels and nets. Large specimens were also preserved in pre-cooled 96% EtOH. For all specimens the ethanol was decanted after 24 hours and replaced with new 96% EtOH to guarantee high ethanol concentration for preservation of high-quality DNA, and subsequently stored at -20°C. In the laboratory at Senckenberg am Meer, Germany,

an integrative molecular-morphological approach was implemented for the identification of the ophiuroid specimens. In total,  
130 DNA was extracted from 525 specimens. For species delimitation analyses 300 sequences were selected (see below). All the  
ROV-collected specimens were photographed on-board, while the EBS-collected specimens were photographed in the lab  
using a Leica binocular stereo-microscope or a Keyence digital microscope, VHX-5000. The voucher specimens are stored in  
Senckenberg am Meer, DZMB, Wilhelmshaven, Germany.

### 2.3 Morphological species identification

135 All ophiuroid individuals collected were morphologically identified to the lowest possible taxonomic level (primary species  
hypotheses, PSH, Puillandre et al., 2012; Boissin et al., 2017). Where possible, individuals were assigned to named species,  
however, in many cases because of their very small size, their early developmental stage (post-larval individuals) or their  
unique morphology, assignment in a morphological operational taxonomic unit was possible only at a higher taxonomic level,  
i.e. genus or family level. For a small number of damaged specimens, morphological identification beyond class was not  
140 possible. Following the DNA analyses (see below), all individuals within the same morphospecies that appeared to be  
genetically distinct from one another were re-examined and if necessary reassigned to different morphospecies, while some  
were considered to be true cryptic species in which clear morphological differences were not identified. Finally, the integrated  
approach allowed the assignment of damaged specimens into different operational taxonomic units. Taxonomic and  
systematic remarks for each SSH are given in the supplementary material.

### 145 2.4 Barcoding data collection

#### 2.4.1 DNA extraction, amplification and sequencing

For the mtDNA COI analyses genomic DNA was extracted from arm tissue in individuals larger than 1–2 mm or from whole  
individuals when smaller than 1–2 mm. DNA extractions were carried out using 30  $\mu$ l Chelex (InstaGene Matrix, Bio-Rad)  
according to the protocol of Estoup et al. (1996) and directly used as DNA template for PCR. All DNA samples were stored  
150 at  $-20^{\circ}\text{C}$ . In the cases where the whole individual was used, 20–25  $\mu$ L of the supernatant was first separated from ophiuroid's  
voucher specimen, while the individual, which was generally intact, was transferred to 96% ethanol and stored as a voucher  
for morphological identifications. A fragment of 657bp of the mitochondrial cytochrome c oxidase subunit (COI) was  
amplified by polymerase chain reaction (PCR). Amplifications were performed using Illustra PuReTaq Ready-To-Go PCR  
Beads (GE Healthcare) in a 25- $\mu$ L volume containing 22  $\mu$ L ddH<sub>2</sub>O, 0.5  $\mu$ L of each primer (10 pmol $\mu$ L<sup>-1</sup>) and 2  $\mu$ L of DNA  
155 template or AccuStart PCR SuperMix (ThermoFisher Scientific) in a 25- $\mu$ L volume containing PCR SuperMix (9.5  $\mu$ L ddH<sub>2</sub>O,  
12.5  $\mu$ L AccuStart), 0.5  $\mu$ L of each primer (10 pmol  $\mu$ L<sup>-1</sup>) and 2  $\mu$ L of DNA template. For the COI amplification the forward  
primer LCOech1aF1 and the reverse primer HCO2198, tailed with M13F and M13R-pUC, respectively (Folmer et al., 1994;  
Layton et al., 2016) were used. The amplification conditions consisted of an initial denaturation step of 3 min at  $94^{\circ}\text{C}$ , 35  
cycles of 30 s at  $94^{\circ}\text{C}$ , 60 s at  $42\text{--}47^{\circ}\text{C}$  and 1 min at  $72^{\circ}\text{C}$ , followed by a final extension step of 5 min at  $72^{\circ}\text{C}$ . All PCR

160 products were purified using ExoSap-IT (ThermoFisher Scientific). The amplified fragments were sequenced in both directions at Macrogen Europe Laboratory (Amsterdam, The Netherlands).

#### 2.4.2 Alignment, genetic divergence

The obtained COI sequences were searched against the GenBank nucleotide database using BLASTN (Altschul et al., 1990). Forward and reverse sequences for each individual were assembled and edited using Geneious v.9.1.7 (www.geneious.com; 165 Kearse et al., 2012). The edited COI sequences were aligned using MAFFT v7.308 under E-INS-i and G-INS-I algorithms (Katoh et al., 2002), while alignments were further manually edited. Our dataset was supplemented with 18 COI ophiuroid sequences from the study of Glover et al. (2016). Sequence data are available in GenBank (Accession numbers XXXXXXXX–XXXXXXX). The sequences, trace files, collection data and photos for each specimen are listed in the datasets CCZ\_Ophiuroidea (doi: xxxxxxx) and DEA\_Ophiuroidea in BOLD (doi: xxxxxxx).

#### 170 2.5 Putative species delimitation

Congruent support across a range of species delimitation approaches is assumedly provides more reliable results than a single method (Carstens et al., 2013; Fontaneto et al., 2015). Therefore, five different species delimitation analyses, including both distance- and tree-based approaches, were performed on the COI dataset, to allocate sequences into genetic species (secondary species hypotheses, SSH; Puillandre et al., 2012; Boissin et al., 2017). Distance-based approaches detect the distance at which 175 the ‘barcode gap’ occurs and sort the sequences into putative species based on this distance, whereas tree-based approaches use a phylogenetic tree from which the fit of speciation and coalescent processes are modelled to delineate species based on the branching rate of the tree (Carstens et al., 2013; Tang et al., 2014).

##### 2.5.1 Distance-based approaches

A neighbour-joining tree was constructed in MEGA7 using a p-distance substitution model, treating gaps/missing data with 180 “pairwise deletion”, and by running 1000 bootstrap replicates. Automatic Barcode Gap Discovery (ABGD) analysis was implemented on the web interface: <http://www.wabi.snv.jussieu.fr/public/abgd/> with default parameters, under the p- distance model (Puillandre et al., 2012). Barcode Index Numbers (BINs) were assigned on the registered DNA dataset automatically using the BOLD v.4 workbench (ww.boldsystems.org; Ratnasingham and Hebert, 2013).

##### 2.5.2 Maximum Likelihood tree

185 The COI barcode data available for all 300 samples was adequate to show genetic diversity patterns within and among closely related species but was not sufficient to accurately reconstruct relationships and genetic distances among the many divergent lineages in this biota. Hence to provide an all barcode sample maximum likelihood tree better reflecting these divergences the barcode samples were appended to a powerful phylogenetic framework: the 48,475-site exon-28SrDNA-COI supermatrix dataset used by Christodoulou et al. (2019). This dataset comprised 200 species that outlined the ophiuroid family-level

190 phylogeny (O'Hara et al., 2017) and 49 CCZ-DEA barcode samples with both COI and 28S sequences included (Christodoulou  
et al., 2019). The COI and 28S allowed the barcode only samples to be linked to the phylogenomic exon data. A maximum  
likelihood tree was constructed by IQ-TREE 1.6.9 (Nguyen et al., 2015; Hoang et al., 2018) using a five partition (exon codon  
positions, 28S, COI) HKY+G model and 1000 ultrafast bootstrap replicates (with NNI optimization). Then the 200  
“supermatrix backbone” samples were pruned out to leave only the 300 barcode samples, node support bootstrap values  
195 recalculated, and the tree rooted according to O'Hara et al. (2017).

### 2.5.3 Tree-based approaches

The General Mixed Yule Coalescent (GMYC; Pons et al., 2006) method was implemented using the R package SPLITS  
(Fujisawa and Barraclough, 2013), under the single-threshold model (stGMYC), and with the required ultrametric tree being  
produced in BEAST v.2.5. Settings were as follows: strict clock, Yule speciation model, GTR+G substitution site model, two  
200 independent MCMC chain runs for 50,000,000 generations, sampled every 1,000 steps (10% was discarded as burn-in period).  
The multi-rate Poisson Tree Processes (mPTP; Kapli et al., 2017) analysis used the rooted “supermatrix backbone” IQ-TREE  
phylogeny (see above). The mPTP was implemented on the web server: <https://mptp.h-its.org> using the multi-rate Poisson tree  
process model and following default settings.

### 2.6 Genetic distances

205 Sequence divergences (Table 1, Tables S1–S2) were estimated using uncorrected p-distances and under the K2P model using  
MEGA7 according to the secondary species hypotheses.

### 2.7 Assemblage structure and diversity analyses

Comparison of the ophiuroid assemblages between areas was performed in R using the package ‘vegan’ (Oksanen et al., 2008).  
As the sampling effort was very different between areas, the species composition table (Table 2), including the specimens of  
210 each species found in each area, was subjected to ‘Chord’ transformation to explore differences in relative abundance and to  
‘presence-absence’ transformation related to faunistic differences. After transformation nMDS ordination was achieved with  
Euclidean distance (Legendre and Gallagher, 2001). As the number of specimens found differs greatly between areas, diversity  
comparison was achieved using rarefaction curves, together with standard diversity indices Shannon ( $H'$ ), Simpson ( $D$ ) and  
Jaccard’s Evenness ( $J$ ). The expected number of species per area was inferred using the extrapolation methods Chao1 (Chao,  
215 1994; Colwell and Coddington, 1994) and ACE (Chazdon et al., 1998). Chao1 uses the proportions of singletons and  
doubletons in the sample to estimate expected species richness, while ACE is an abundance-based coverage estimator. For the  
analysis of beta (regional) diversity, the total multiple-site beta diversity  $\beta_{\text{SOR}}$  was calculated using the modified Sørensen Index  
(Sørensen, 1948; Balseaga and Orme, 2012), and  $\beta_{\text{SOR}}$  was decomposed into its additive components “multiple-site species  
turnover”  $\beta_{\text{SIM}}$  (Simpson Index: Simpson, 1943) and “multiple-site nestedness”  $\beta_{\text{SNE}}$  using the R package “betapart” (Balseaga,  
220 2010; Balseaga and Orme, 2012). In order to explore the relative contribution of every area to species turnover and nestedness,

these values were calculated taking one area out each time in a jackknife approach. Changes in turnover and nestedness were then attributable to the area that was excluded from the analysis.

### 3 Results

#### 3.1 Species delineation

225 The species delineation data set was comprised of 300 barcode sequences (Fig. 2), out of which 287 were novel sequences (BOLD datasets: CCZ\_Ophiuroidea, DEA\_Ophiuroidea), ranging from 547 to 657bp in length (92% has 657bp length). Both trees produced by neighbour-joining, NJ (Fig. 2) and Maximum Likelihood, ML (Fig. 3) showed a broad pattern in which SSH were separated by long branches, while branches within species were shorter. The three hundred DNA barcodes clustered into 42 monophyletic clades in NJ and into 40 in ML supported by high bootstrap values (>90).

230 The ABGD analysis yielded a total of 35 SSH based on initial partitioning over the range of prior values for maximum intraspecific divergence (Fig. 2, Fig. S1). Identical results were produced based on JC69 and K80 corrected distances. The number of SSH varied between 37 and 50 after the application of recursive partitioning. Low threshold values of 0.0010–0.0028 and 0.0046–0.0077 prompted 50 and 47 SSH respectively (Fig. S1). Moderate threshold values of 0.0129 and 0.0215 resulted in 43 and 42 SSH, respectively (Fig. S1). Finally, higher prior threshold values of 0.0359–0.0599, and 0.1000 provided

235 40 and 37 SSH, respectively (Fig. S1). To be conservative, we focus primarily on the results of initial partitioning (35 SSH) as they were consistent across the parameter settings and congruent with other species delimitation methods (Puillandre et al., 2012; Kekkonen and Hebert, 2014). Nevertheless, for comparative reasons, the results of the recursive partition with prior divergence 0.0359–0.0599 and which suggested 40 SSH are also presented here (Fig. 2, Fig. S1).

In BOLD, the 300 barcodes were assigned to 49 BINs (Fig. 2), of which 22 BINs had a single record and 3 BINs had two

240 records (CCZ\_Ophiuroidea DEA and Ophiuroidea datasets, BOLD). Single-threshold general mixed Yule-coalescent calculations (stGMYC) yielded 47 SSH (entities) with a confidence interval ranging from 46 to 49 (Supplementary Material, Result of GMYC). The mPTP model produced a more conservative number of clusters (42 SSH) compared to the GMYC method (Supplementary Material, Results of mPTP).

245 Depending on the applied method, the numbers of different putative species ranged from 35 to 49. Arranging the implemented methods by increasing conservativeness gives the following: BINs (49) < stGMYC (47) < mPTP (42) < ABGD (35). In the present study a consensus dataset of species that were delineated by at least three of the four above-mentioned approaches was selected, as species delineation methods tend to overestimate the number of species present in a dataset. In the few cases that the methods were inconsistent, the most conservative approach was adopted after taking into account the genetic distance

250 between the potential species. The results were cross-referenced with the topology produced by both the NJ and ML trees. It is worth mentioning that 27 SSH were congruent throughout all methods and 34 SSH were consistent when excluding ABGD<sub>i</sub> (initial) which was the most conservative method. In total 43 SSH were recovered from the CCZ and the DEA, of which some

were PSHs splitted from two up to five SSHs each. Noticeably, the PSHs *Amphioplus daleus*, *Ophiuroglypha cf. polyacantha* and *Ophiosphalma glabrum*, *Ophiocymbium* sp. revealed cryptic lineages between their populations in the CCZ and the DEA. The 43 SSHs (Figs 5–16) are grouped in 11 families, Amphilepididae, Amphiuridae, Euryalidae, Ophiernidae, Ophiohelidae, Ophiolepididae, Ophioleucidae, Ophiopyrgidae, Ophioscolecidae, Ophiosphalmidae, Ophiotomidae, attributed to all the current ophiuroid orders (Fig. 3), Amphilepidida, Euryalida, Ophiacanthida, Ophioscolecida, Ophiurida (see also Taxonomic and systematic remarks, Supplementary Material).

### 3.2 Genetic distances

Summaries of uncorrected pairwise distances for the ophiuroid species (SSHs) are shown in Table 1 and Fig. 4, with the full data available in the Supplementary Material Section (Table S1–S2). Mean interspecific genetic distances ranged from 0.050 to 0.370 (p-distance) and 0.052 to 0.512 (K2P distance) with the lowest divergence value observed between *Ophiosphalma glabrum* and *Ophiosphalma cf. glabrum* (Species 3 vs 36) and the highest between *Ophiacantha cosmica* (Species 27) and *Ophiohelidae* sp. (Species 32). Mean intraspecific variability ranged from 0.00 to 0.055 (p-distance) and 0.00 to 0.057 (K2P distance), with the highest values observed in the ophiuroid *Amphioplus cf. daleus*. It should be mentioned that there were 13 SSHs represented by only one sample (singletons).

### 3.3 Ophiuroid assemblages and diversity

The species composition table (Table 2) shows the counts of each species by area. The diversity values are summarised in Table 3. A total of 55 sites were sampled in seven areas. Sampling effort was uneven, with most samples deriving from the BGR area (18) and the DEA (14) in the Peru Basin. For all other areas, 3–6 sites were sampled. A total of 543 specimens were assigned to the 43 species. None of the species was recorded in all seven areas, while the most common species were Species 29 (Ophioleucidae), Species 2 (*Amphioplus daleus*) and Species 3 (*Ophiosphalma glabrum*) which were found in 6 areas, all of them absent in APEI3. It is worth mentioning that the majority of species (44.2 %) was present only in one of the area (19 SSHs). Highest species numbers were found in the BGR and UKSRL areas (24 and 21 respectively), where also the highest number of specimens were recorded (219 and 158 respectively). Lowest values were found in the IFREMER area, with 13 specimens being attributable to 5 species. While the number of species was a function of the number of specimens, less species were recorded in the IFREMER and IOM areas than would be expected if they were to follow the same pattern as at other sites (Fig. 17). This was corroborated by the rarefaction analysis (Fig. 18), which shows that for the same number of specimens, the IFREMER and IOM areas have fewer species. The rarefaction curves of all other areas were very similar. Low diversity in the IFREMER and IOM areas was also indicated by the lowest Shannon Diversity, Simpson Diversity and Evenness values, while highest diversity values were recorded in the areas UKSRL, BGR and DISCOL (Table 4). The extrapolation analyses predicted a total of 57 species (Chao1 index) and 53.5 species (ACE index) for all areas together. Lowest extrapolated numbers of species were again obtained for the IFREMER and IOM areas (6.5–12 and 8.5–11.5, respectively), whereas highest numbers were obtained for the BGR and UKSRL areas (57–51.1 and 27.2–30.5, respectively). The highest number of unique species (species

285 found only in one area) was found in the areas BGR (6 species), UKSRL (5 species) and APEI3 (5 species), while no unique species were observed in the IFREMER and GSR areas.

The faunistic similarity is summarised in Table 4, showing the number of shared and unshared species between areas. APEI3 showed the lowest numbers of shared species (0–2) and the highest number of unshared species (13–32) compared with other areas. The most distant area, DISCOL in the Peru basin, shared 3–11 species with CCZ exploration areas, but none with APEI3.  
290 Beta diversity decomposition is shown in Fig. 19. The total multiple-site beta diversity was high ( $\beta_{\text{SOR}}=0.782$ ), with a higher component of turnover ( $\beta_{\text{SIM}}=0.640$ ) versus nestedness ( $\beta_{\text{SNE}}=0.142$ ). To explore the relative contribution of each area to total beta diversity, each area was taken out once and beta diversity was re-calculated. The relative change in turnover and nestedness was then attributable to the omitted area. Results of this exercise are shown graphically in Fig. 19 and numerically in Table 4. Removing most of the areas one by one (excluding APEI3) did not result in a drastic change in turnover and  
295 nestedness ( $\beta_{\text{SIM}}=0.604\text{--}0.663$ ;  $\beta_{\text{SNE}}=0.121\text{--}0.177$ ). Only the exclusion of APEI3 resulted in a substantial reduction of turnover and increase of nestedness ( $\beta_{\text{SIM}}=0.488$ ;  $\beta_{\text{SNE}}=0.229$ ).

The nMDS plot in Fig. 20 shows the quantitative assemblage analysis using Chord distance (relative abundance). The BGR and UKSRL areas were close together, but also close to the areas of DISCOL, IFREMER and IOM, while greater dissimilarity occurs with the GSR and APEI3 areas. The boxplot in Fig. 21 shows the variation in Chord distance of each area to other areas,  
300 evidencing that APEI3 was most different to any other area (see median and extent of whiskers) than other areas between each other.

The ordination using presence/absence transformed data placed the areas with less unique species (IFREMER, GSR and IOM) in the middle of the plot and spreaded the areas with highest number of unique species at the outer margins and apart from each other (Fig. 22). The boxplot in Fig. 23 shows that APEI3 was the most dissimilar in terms of presence/absence of species,  
305 but the median value (black horizontal bar inside the boxes) was as high as UKSRL and BGR areas, which, however, displayed less variation.

## 4 Discussion

### 4.1 Species delimitation method performance

The results obtained here were consistent with many other studies showing that different species delimitation methods can  
310 produce different delimitation scenarios when employing single-locus data (Hofmann et al., 2019). The single-locus species delimitation methods tested here, although they are extensively used throughout the literature, including for the Ophiuroidea (Khodami et al., 2014; Laakman et al., 2016; Boissin et al., 2017), are each subject to potential biases and differing conditions inherent in the empirical datasets (Hofmann et al., 2019). The five species delimitation methods used here generally recovered the same number of SSH and despite some degree of incongruence observed in the numbers of SSHs, they were consistent in  
315 recovering more SSHs than the number of species originally recognised. Given the lack of information regarding the biodiversity and of the relationships between deep-sea ophiuroids, it was not surprising that more lineages were inferred than

are currently recognised. It is likely that many of these SSHs correspond to undescribed cryptic species, but simultaneously some may be the result of genetic drift or isolated populations currently undergoing speciation. Noticeably, the BIN method in BOLD recovered a higher number of species than all other approaches. BOLD and specifically BINs can greatly improve the Linnaean taxonomic assignment in many animal groups, including echinoderms (Layton et al., 2016; Laakman et al., 2016). The low intra-cluster divergence (2.2%) at the initial cluster step of RESL methodology (Ratnasingham and Hebert, 2013; Song et al., 2018) could be the reason why, in some cases the BIN method overestimated species number, especially since there appears a small overlap between intraspecific and interspecific distance in our data (Fig. 4). This could be the case in the delimited *Ophiocymbium* spp. (species 24, 25, 40; Fig. 2, Table S2), which were separated into numerous lineages despite the relative low divergence between them. Generally, barcodes are well defined when the lowest interspecific distance exceeds the highest intraspecific distance, and in such cases a species delineation ‘threshold’ will be clear. But, as the threshold can be lineage-specific, a universal threshold that fits all the branches may not exist, as coalescent depths among species will vary greatly due to differences in population size, mutation rate and speciation times (Colins and Cruickshank, 2012). Similarly, GMYC recovered a relatively high number of species (47 vs 49 BINs). Arguably, GMYC and especially the single-threshold version of the method is a robust species delimitation method (Fujisawa and Barraclough, 2013). GMYC performance depends on a single-locus ultrametric tree which tends to compress the coalescent events towards the tips of the tree, making it especially difficult to distinguish closely related species (Boissin et al., 2017). It has been argued that the PTP methods generate diversity estimates that are more robust to different phylogenetic methods, while GMYC is more sensitive, but provide consistent estimates for BEAST trees (Tang et al., 2014). Nevertheless, unresolved nodes can affect both GMYC and PTP estimates, although seem to have a greater effect on GMYC estimates (Tang et al., 2014). In contrast it seems that ABGD (initial partition) has underestimated the species number in this study, although the performance of the method improved when the recursive partition option was used. ABGD has been reported to over-lump speciose datasets with high speciation rates (Dellicour and Flot, 2018). ABGD’s conservatism and GMYC’s overestimation have also been shown on reef brittle stars (Boissin et al., 2017), while both studies indicated that PTP methods show a small advantage as the most stable, suggesting the presence of additional cryptic species but without over-splitting taxa. Summarising, despite the differences in the number of delimited species, overall the methods recovered a broadly similar number of SSH. Congruence among different delimitation methods is a strong indication that the delimitation is correct, allowing the designation of cryptic species and rectification of taxonomic problems (Dellicour and Flot, 2018), always when possible taking into account the morphology.

#### 4.2 Taxonomic Implications

The abyssal Eastern Pacific harbours a highly diverse ecosystem. The number of ophiuroid species reported from the polymetallic nodule fields of the Pacific has now increased by 433%, from 10 (Glover et al., 2016; Amon et al., 2017) to 43 in this paper. This is the largest collection of any megafaunal taxon in the CCZ and the only one that has been studied in such detail using a comprehensive combination of morphological and genetic evidence. Remarkably, from the species reported here, 32 (75%) are probably new to science and some represent hitherto unknown old evolutionary lineages (see also Christodoulou

350 et al., 2019). The discovery of new species is the direct result of increased sampling effort, in which a greater number of specimens deriving from a larger sampling surface were collected than during any previous studies in the DEA or in CCZ, spanning over five exploration contract areas and one APEI. Furthermore, the use of new sampling gears, i.e. Epibenthic Sledge (EBS), in relation to past historical expeditions that took place in the area, permitted the collection of fragile and minute specimens, while new DNA barcoding approaches allowed the identification of post-larvae and juveniles that lacked adult  
355 morphological characters. Overall, these data show that the brittle-star biodiversity in the deep sea is still greatly underestimated, while supporting the use of DNA barcoding as an effective and time-efficient method of species delimitation to complement morphological studies. Although we do not wish to suggest that single mitochondrial locus data should be used on its own to draw taxonomic conclusions, in much the same way as using single morphological characters is discouraged (DeSalle, 2006; Hofman et al., 2019), we do argue that single gene barcoding, could be the first step in identifying previously  
360 overlooked species, while also providing a guide in cases where morphological identification is difficult. It was only recently that a transcriptome-based analysis of Ophiuroidea (O'Hara et al., 2014) instigated a major re-evaluation of morphology-based classifications (Smith et al., 1995), proving that there is still a lot to be discovered and re-evaluated within this group. Specifically in our study, DNA barcoding proved to be necessary since a significant proportion of the specimens are post-larvae juveniles, making their identification based on morphological characteristics quite challenging. DNA barcoding not  
365 only allowed species delimitation but also aided in matching post-larvae individuals with their corresponding adults, as for example in the case of *Ophiosphalma glabrum* where individuals ranging from 0.5 mm to 20 cm were collected (Fig. 23). Furthermore, the large-sized brittle-stars collected with the remotely operated vehicle were matched with their in-situ photos allowing a more accurate estimation of morphospecies which in turn could facilitate the more accurate annotation of photos and video transects used in various biodiversity assessment studies (Tilot et al., 2018)

370 Mean COI genetic intraspecific distances (K2P) of brittle stars (0.00–0.057) were concordant with previous ophiuroid studies (0.00–0.042: Khodami et al., 2014 and 0.00–0.064: Boissin et al., 2017), while the mean COI interspecific genetic distances (0.052–0.512) were found to be noticeably higher. This could be attributed both to the great phylodiversity of ophiuroids collected from the polymetallic fields, spanning over 11 families and 5 orders, and to the discovery of previously undescribed diversity up to the family level (Christodoulou et al., 2019).

### 375 **4.3 Ophiuroid diversity and assemblage structure, implications for conservation in the light of possible nodule mining**

Mining of abyssal polymetallic nodules in the CCZ could result in severe habitat disruption and loss of benthic communities in and directly around the mined sites (Vanreusel et al., 2016). An attempt to foresee the potential impact of deep-sea mining to abyssal communities requires a profound knowledge of natural background biodiversity and ecosystem functioning, such as how many and which species are living there now? How large are the species ranges? Are there natural changes in diversity  
380 along environmental gradients? However, our knowledge of abyssal benthic communities is still so poor, that even these simple questions remain unanswered for many groups of organisms in what is nonetheless considered to be an economically important

and potentially endangered deep-sea region like the CCZ. We can now provide partial answers to these questions for the ophiuroids, one of the dominant megafaunal groups in the CCZ.

Our initial assumption was that ophiuroid diversity would be low (we expected around 10 species) based on the previous studies in the region (Glover et al., 2016; Amon et al., 2017) and on a recent review of global ophiuroid distribution, in which only 28 species were recorded for the whole tropical East Pacific at abyssal depths (Stöhr et al., 2012). Coupled with expectations of low diversity we assumed that connectivity would be high and that most beta diversity between sites would be composed of nestedness (high) rather than species turnover (low). Under these circumstances, the APEI3 could be a good region to host most of the CCZ species and serve as source for most of the populations. Also we assumed that the most distant DISCOL area would display a low similarity with the CCZ.

The results of our study do not support any of these initial assumptions, in fact, they show exactly the opposite. We recorded a fourfold higher number of species than expected and rarefaction curves show no sign of reaching an asymptote (Fig. 18). Chao1 and ACE estimators predicted between 53 and 57 species across the region (Table 4). The ophiuroid communities were characterised by high beta diversity that is mainly composed of high turnover between areas, rather than nestedness. This means that there was a high proportion of rare species (19 species were present in only one area and 12 species in only in 2 areas), which reduces nestedness and increases the potential for damage to natural populations caused by deep-sea mining at local scale. Food availability regulated by particulate organic carbon (POC) flux seems to strongly influence diversity and abundance in abyssal ecosystems (Smith et al., 2008). The CCZ licence areas for exploration despite being all in a mesotrophic zone are not all the same. The POC flux in the CCZ shows a southeast to northwest gradient increasing towards its eastern edge (Vanreusel et al., 2016; Volz et al., 2018, in press). Volz et al. (2018, in press) after studying four of the CCZ areas studied herein and the APEI3 found that they differ in POC fluxes to the seafloor ranging from as low as  $1 \text{ mg C}_{\text{org}} \text{ m}^{-2} \text{ d}^{-1}$  in APEI3 to  $2 \text{ mg C}_{\text{org}} \text{ m}^{-2} \text{ d}^{-1}$  to BGR area. Within this study the highest diversity values were recorded in the areas UKSRL, BGR and DISCOL. The BGR and UKSRL areas are located in the far east of CCZ, in a region of higher POC flux (Vanreusel et al., 2016; Volz et al., 2018, in press), that could explain higher standing stocks and higher species diversities and abundances. Food availability seems to justify why the communities of the very distant and eutrophic DISCOL area (Haeckel et al., 2001), resemble the eastern CCZ more than the geographically closer APEI3. The DISCOL area shares 11 species with the BGR and 8 species with the UKSRL area, while no species are shared with APEI3. In contrary to the CCZ areas APEI3 lies within an oligotrophic zone exhibiting twofold lower POC fluxes and subsequently twofold lower aerobic respiration rates in comparison to the BGR area (Volz et al., 2018, in press). APEI3 differs significantly from the rest areas in additional aspects such as lower Chloroplasic Pigment Equivalent (CPE) and total organic carbon (TOC) values, lower sedimentation rates resulting in finer sediments, with higher clay content (Hauquier et al., 2019; Volz et al., 2018, in press). In conclusion the APEI3 biogeochemical features differ considerably from the other areas (Volz et al., 2018, in press) and could explain the fact that APEI3 has a very different assemblage sharing only up to two species with the CCZ areas and DISCOL. Furthermore, APEI3 is mainly located outside the CCZ, north of the Clarion Fracture, a submarine mountain range characterised by a peak and trough surpassing 1800 m difference in elevation (Hall and Gurnis, 2005), which may act as a dispersal barrier for abyssal fauna.

This raised the critical question whether the APEI3 fauna is representative for the exploration licence areas in the CCZ especially as ISA created the APEIs based on environmental conditions but in the absence of any biological data (Wedding et al., 2013). Our results suggest that APEI3 may not be a good surrogate area for the CCZ nodule fauna. Only a small fraction of the total registered ophiuroid fauna was recorded in APEI3. This area is the most different in terms of species composition and assemblage structure (Figs 17, 19). Removing the APEI3 from beta analysis, results in a great reduction of turnover and increase of nestedness. This means that the remaining areas become more similar to each other, the total beta diversity decreases, and differences between sites due to missing species out of a common species pool (nestedness) increases when APEI3 is excluded. Lower species richness and abundance in APEI3 as well as very low similarity between the APEI3 and the exploration areas, independently of distance were also found in the studies of Vanreusel et al. (2016), Hauquier et al. (2019) and Bonifácio et al. (in press) after studying megafaunal, nematode and polychaete assemblages respectively. Volz et al. (2018, in press) after studying the (bio)geochemical characteristics of APEI3 as well as four eastern CCZ concluded that the preservation area APEI3 does not represent the depositional conditions and bio-geochemical processes that are dominating in the investigated CCZ license areas. The results of these studies converge with ours in finding that APEI3 is ill-suited as representative area of the recovery of the potentially mined areas. Furthermore, Taboada et al. (2018) found that APEI6 is inadequate to act as population source for a hexactinellid sponge species and suggest the designation of a new APEI closer to the exploration areas studied. The large geographic distance between the APEIs and the explorations areas, may hinder the exchange of individuals and the genetic flow, among remaining populations after mining. Therefore, we strongly advocate in favour of incorporating no-mining sites within the core CCZ area, having a similar nodule composition as the potential mining areas, rather only in the periphery of CCZ, as was already suggested by Vanreusel et al. (2016), in order to prevent the loss of biodiversity.

Biodiversity studies that focus only on known, nominal species are problematic, as they likely overlook cryptic or undiscovered lineages involved in diversification. As shown herein, most of the brittle stars recorded in the CCZ and Peru Basin lack formal Linnaean scientific names, thus widening the gap between described species and actual biodiversity, which appears to be far greater than previously estimated. Not recognising these cryptic or undescribed taxa ensures that they remain in the shadows of research and conservation policies. These taxa could be locally endemic or rare, and thus more vulnerable to human impacts such as deep-sea mining. Biodiversity studies, such as presented here, aiming to develop reference libraries while using an integrative taxonomic approach, such as presented here, will provide much-needed comprehensive and time-efficient assessments of “missed” diversity. These, in turn, may fill the gaps for adequate baseline assessment at the onset of commercial-scale mining and thus, through adequate management schemes, prevent serious species declines before they have been adequately described or even discovered.

In conclusion, it is important to note that present study explored only a part of the polymetallic fields of the CCZ and DEA. Our dataset on ophiuroid communities in the CCZ is the largest available to date, but still too small to allow for comprehensive conclusions. The conclusions for APEI3 cannot be extrapolated to other APEIs in the region. Also, our dataset is biased toward the eastern areas of the CCZ where the sampling effort was higher. Thus, although a large number of specimens were examined,

450 is highly likely that the true biodiversity is even much higher. Broader efforts, especially those that will include samples from the western parts of the CCZ, or from other APEIs, are likely to result in the discovery of additional diversity and will allow us to obtain a better understanding of connectivity and patterns of distribution across the CCZ. This will in turn refine our perception of the marine biodiversity of the abyssal plains and specifically of polymetallic nodule fields.

## 5 Conclusions

455 Five methods of species delineation showed concordant results and revealed 43 deep-sea ophiuroid species in the Clarion-Clipperton Zone and the DISCOL Experimental Area (Pacific Ocean), revealing an unexpectedly high diversity and showing that the most conspicuous invertebrates in abyssal plains have been so far considerably under-estimated. This study increases the number of ophiuroid species reported from polymetallic nodule fields of the Pacific by 433%.

A comprehensive reference library including 287 novel ophiuroid sequences allocated to 43 species is produced. This reference  
460 library can facilitate the assessment of potential impacts and biodiversity loss due to deep-sea mining. It is the first time such an integrated reference library is produced for the CCZ and the DISCOL area including both genetic and morphological information about the most emblematic mobile megafaunal inhabitants.

The biodiversity patterns observed within CCZ could be mainly attributed to differences in POC fluxes explaining the higher species numbers found in BGR and UKSRL areas. The five exploration contract areas belong to a mesotrophic province, while  
465 in contrary the APEI3 (Area of Particular Environmental Interest) is located in an oligotrophic province which could explain the lowest diversity as well as very low similarity with the other six study areas.

Based on the results of our study the representativeness and the appropriateness of APEI3 (Area of Particular Environmental Interest) to meet its purpose of preserving the biodiversity of the CCZ fauna is questioned, while the creation of no-mining sites within the core CCZ area is suggested.

## 470 Data availability

DNA sequences, trace files, collection data and taxonomic remarks are available in the datasets CCZ\_Ophiuroidea and DEA\_Ophiuroidea in BOLD. Furthermore, the DNA sequences and their accompany collection data are also available in GenBank.

## Author contribution

475 PMA and AV designed the sampling. PMA, AV, SK, CFR and AH carried out the sampling and processed the specimens on board. MC performed the sequencing program. AFH performed the phylogeonomic analyses. MC, TO'H, AFH, CFR and PMA

analysed and interpreted the data. MC took the lead in writing the manuscript in collaboration with TO'H and PMA, to which all other authors contributed.

### Competing interests

480 The authors declare that they have no conflict of interest.

### Acknowledgments

The authors will like to thank Carsten Rühlemann (Federal Institute for Geosciences and Natural Resources, BGR, Hannover) for making the material from the BGR cruises BIONOD, MANGAN 2013 and MANGAN 2014 available. The cruises SO239 and SO242 were financed by the German Ministry of Education and Science (BMBF) as a contribution to the European project  
485 JPI Oceans “Ecological Aspects of Deep-Sea Mining”. The authors acknowledge funding from BMBF under Contract 03F0707E. The ABYSSLINE cruises were funded by UK Seabed Resources Ltd. Thanks are due to Foundation for Science and Technology, Ministry of Science, Technology and Higher Education (FCT/MCTES) for the financial support to CESAM (UID/AMB/50017/2019), through national funds. The author C.F. Rodrigues was funded by national funds (OE), through  
490 FCT, I.P., in the scope of the framework contract foreseen in the numbers 4, 5 and 6 of the article 23, of the Decree-Law 57/2016, of August 29, changed by Law 57/2017, of July 19.

### References

- Altschul, S. F., Gish, W., Miller, W., Myers, E. W., and Lipman D. J.: Basic local alignment search tool, *J. Mol. Biol.*, 215, 403–410, doi: [10.1016/S0022-2836\(05\)80360-2](https://doi.org/10.1016/S0022-2836(05)80360-2), 1990.
- Amon, D. J., Ziegler, A. F., Dahlgren, T. G., Glover, A. G., Goineau, A., Gooday, A. J., Wiklund, H., and Smith C. R.: Insights  
495 into the abundance and diversity of abyssal megafauna in a polymetallic-nodule region in the eastern Clarion-Clipperton Zone, *Sci. Rep.*, 6, 30492, doi: [10.1038/srep30492](https://doi.org/10.1038/srep30492), 2016.
- Amon, D. J., Ziegler, A. F., Kremenetskaia, A., Mah, C. L., Mooi, R., O'Hara, T., Pawson, D. L., Roux, M., and Smith C. R.: Megafauna of the UKSRL exploration contract area and eastern Clarion-Clipperton Zone in the Pacific Ocean: Echinodermata, *Biodivers. Data J.*, 5, e11794, doi: [10.3897/BDJ.5.e11794](https://doi.org/10.3897/BDJ.5.e11794), 2017.
- 500 Baselga, A.: Partitioning the turnover and nestedness components of beta diversity, *Glob. Ecol. Biogeogr.*, 19, 134–143, doi: [10.1111/j.1466-8238.2009.00490.x](https://doi.org/10.1111/j.1466-8238.2009.00490.x), 2010.
- Baselga, A., and Orme, C. D. L.: betapart: an R package for the study of beta diversity, *Methods Ecol. Evol.*, 3, 808–812, doi: [10.1111/j.2041-210X.2012.00224.x](https://doi.org/10.1111/j.2041-210X.2012.00224.x), 2012.

- Boissin, E., Hoareau, T. B., Paulay, G., and Bruggemann, J. H.: DNA barcoding of reef brittle stars (Ophiuroidea, Echinodermata) from the southwestern Indian Ocean evolutionary hot spot of biodiversity, *Ecol Evol.*, 7, 11197–11203, doi: [10.1002/ece3.3554](https://doi.org/10.1002/ece3.3554), 2017.
- Bonifacio, P., Martinez-Arbizu, P., and Menot, L.: Alpha and beta diversity patterns of polychaete assemblages across the nodule province of the Clarion-Clipperton Fracture Zone (Equatorial Pacific), *Biogeosciences Discuss*, doi: 10.5194/bg-2019-255, in review, 2019.
- 510 Brenke, N.: An epibenthic sledge for operations on marine softbottom and bedrock, *Mar. Technol. Soc. J.*, 39, 13–24, doi: [10.4031/002533205787444015](https://doi.org/10.4031/002533205787444015), 2005.
- Calas, G.: Mineral resources and sustainable development, *Elements*, 13, 301–306, doi: [10.2138/gselements.13.5.301](https://doi.org/10.2138/gselements.13.5.301), 2017.
- Carney, R. S.: Zonation of deep biota on continental margins, in: *Oceanography and Marine Biology: An Annual Review* 43, edited by: Gibson, R. N., Atkinson, R. J. A. and, Gordon, J. D. M., CRC Press, Boca Raton U.S.A., 211–278, doi: [10.1201/9781420037449](https://doi.org/10.1201/9781420037449), 2005.
- 515 Carstens, B. C., Pelletier, T. A., Reid, N. M., and Satler, J. D.: How to fail at species delimitation, *Mol. Ecol.*, 22, 4369–4383, doi: [10.1111/mec.12413](https://doi.org/10.1111/mec.12413), 2013.
- Chao, A.: Non-parametric estimation of the number of classes in a population, *Scand. J. Stat.* 11, 265–270, 1984.
- Chazdon, R. L., Colwell, R. K., Denslow, J. S., and Guariguata M. R.: Statistical methods for estimating species richness of woody regeneration in primary and secondary rain forests of NE Costa Rica, in: *Forest biodiversity research, monitoring and modeling: Conceptual background and Old World case studies*, edited by: Dallmeier, F., and Comiskey, J. A., Parthenon Publishing, Paris, France, 285–309, 1998.
- 520 Christodoulou, M., O'Hara, T. D., Hugall, A. F., and Martinez Arbizu, P.: Dark ophiuroid biodiversity in a prospective abyssal mine field, *Curr. Biol.*, 29, 1–4, doi: [10.1016/j.cub.2019.09.012](https://doi.org/10.1016/j.cub.2019.09.012), 2019.
- 525 Clark, H. L.: North Pacific Ophiurans in the collection of the United States National Museum, *Bull. U. S. Natl. Mus.*, 75, 1–302, 1911.
- Clark, A. H.: Ophiuroidea of the Hawaiian Islands, *Bernice P. Bishop Mus. Bull.*, 195, 14–15, 1949.
- Colins, R. A., and Cruickshank, R. H.: The seven deadly sins of DNA barcoding, *Mol. Ecol. Resour.*, 13 969–75, doi: [10.1111/1755-0998.12046](https://doi.org/10.1111/1755-0998.12046), 2012.
- 530 Colwell, R. K., and Coddington, J. A.: Estimating terrestrial biodiversity through extrapolation, *Phil. Trans. R. Soc. Lond. B*, 345, 101–118, doi: [10.1098/rstb.1994.0091](https://doi.org/10.1098/rstb.1994.0091), 1994.
- Danovaro, R., Aguzzi, J., Fanelli, E., Billett, D., Gjerde, K., Jamieson, A., Ramirez-Llodra, E., Smith, C. R., Snelgrove, P. V. R., Thomsen, L., and Dover, C. L.: An ecosystem-based deep-ocean strategy, *Science*, 355, 452–454, doi: [10.1126/science.aah7178](https://doi.org/10.1126/science.aah7178), 2017.
- 535 Dellicour, S., and Flot, J.-F.: The hitchhiker's guide to single-locus species delimitation, *Mol. Ecol. Resour.*, 18, 1234–1246, doi: [10.1111/1755-0998.12908](https://doi.org/10.1111/1755-0998.12908), 2018.

- DeSalle, R.: Species discovery versus species identification in DNA barcoding efforts: response to Rubinoff, *Conserv. Biol.*, 20, 1545–1547, doi: [10.1111/j.1523-1739.2006.00543.x](https://doi.org/10.1111/j.1523-1739.2006.00543.x), 2006.
- Estoup A., Largiader C. R., Perrot E., and Chourrout D.: Rapid one-tube DNA extraction for reliable PCR detection of fish polymorphic markers and transgenes. *Mol. Mar. Biol. Biotechnol.*, 5, 295–298, 1996.
- Folmer, O. M., Black, W., and Hoen, R.: DNA primers for amplification of mitochondrial cytochrome c oxidase subunit I from diverse metazoan invertebrates, *Mol. Mar. Biol. Biotechnol.*, 3, 294–299, 1994.
- Fontaneto, D., Flot, J. F., and Tang, C. Q.: Guidelines for DNA taxonomy, with a focus on the meiofauna, *Mar. Biodivers.*, 45, 433–451, doi: [10.1007/s12526-015-0319-7](https://doi.org/10.1007/s12526-015-0319-7), 2015.
- 545 Fujisawa, T., and Barraclough, T. G.: Delimiting species using single-locus data and the Generalized Mixed Yule Coalescent approach: a revised method and evaluation on simulated data sets, *Syst. Biol.*, 62, 707–724, doi: [10.1093/sysbio/syt033](https://doi.org/10.1093/sysbio/syt033), 2013.
- Gage, J. D., and Tyler, P. A. (Eds.): *Deep-Sea Biology: A Natural History of Organisms at the Deep-Sea Floor*, Cambridge University Press, Cambridge, United Kingdom, 1991.
- Glover, A. G., Wiklund, H., Rabone, M., Amon, D. J., Smith, C. R., O'Hara, T. D., Mah, C. L., and Dahlgren, T. G.: Abyssal fauna of the UK-1 polymetallic nodule exploration claim, Clarion-Clipperton Zone, central Pacific Ocean: Echinodermata, *Biodivers. Data J.*, 4, e7251, doi: [10.3897/BDJ.4.e7251](https://doi.org/10.3897/BDJ.4.e7251), 2016.
- Haeckel, M., Köönig, I., Riech, V., Weber, M. E., and Suess, E.: Pore water profiles and numerical modelling of biogeochemical processes in Peru Basin deep-sea sediments. *Deep-Sea Res. Part II* 48: 3713–3736, doi: [10.1016/S0967-0645\(01\)00064-9](https://doi.org/10.1016/S0967-0645(01)00064-9), 2001.
- 555 Hall, C. E., and Gurnis, M.: Strength of fracture zones from their bathymetric and gravitational evolution, *J. Geophys. Res. Solid Earth*, 110, doi: [10.1029/2004JB003312](https://doi.org/10.1029/2004JB003312), 2005.
- Hauquier, F., Macheriotou, L., Bezerra, T. N., Egho, G., Martinez Arbizu, P., and Vanreusel, A.: Geographic distribution of free-living marine nematodes in the Clarion-Clipperton Zone: implications for future deep-sea mining scenarios, *Biogeosciences*, 16, 3475–3489, doi: [10.5194/bg-16-3475-2019](https://doi.org/10.5194/bg-16-3475-2019), 2019.
- 560 Hein, J., Mizell, K., Koschinsky, A., and Conrad, T.: Deep-ocean mineral deposits as a source of critical metals for high- and green-technology applications: comparison with land-based resources, *Ore Geol. Rev.*, 51, 1–14, doi: [10.1016/j.oregeorev.2012.12.001](https://doi.org/10.1016/j.oregeorev.2012.12.001), 2013.
- Hoang, D. T., Chernomor, O., von Haeseler, A., Minh, B. Q., and Vinh L. S.: UFBoot2: Improving the ultrafast bootstrap approximation, *Mol. Biol. Evol.*, 35, 518–522, doi: [10.1093/molbev/msx281](https://doi.org/10.1093/molbev/msx281), 2018.
- 565 Hofmann, E. P., Nicholson K. E., Luque-Montes, I. R., Köhler, G., Cerrato-Mendoza C. A., Medina-Flores M., Wilson L. D., and Townsend J. H.: Cryptic diversity, but to what extent? Discordance between single-locus species delimitation methods within mainland anoles (Squamata: Dactyloidae) of Northern Central America. *Front. Genet.*, 10, 11, doi: [10.3389/fgene.2019.00011](https://doi.org/10.3389/fgene.2019.00011), 2019.
- Jamieson, A. (Ed): *The Hadal Zone. Life in the deepest oceans*, Cambridge University Press, Cambridge, United Kingdom, 570 2015.

- Jamieson, A. J. Fujii, T., Mayor, D. J., Solan, M., and Priede, I. G.: Hadal trenches: the ecology of the deepest places on Earth, *Trends Ecol. Evolut.*, 25, 190–197, doi: [10.1016/j.tree.2009.09.009](https://doi.org/10.1016/j.tree.2009.09.009), 2009.
- Kapli, P., Lutteropp, S., Zhang, J., Kobert, K., Pavlidis, P., Stamatakis, A., and Flouri, T.: Multi-rate Poisson tree processes for single-locus species delimitation under maximum likelihood and Markov chain Monte Carlo, *Bioinformatics*, 33, 1630–1638, doi: [10.1093/bioinformatics/btx025](https://doi.org/10.1093/bioinformatics/btx025), 2017.
- Katoh, K., Misawa, K., Kuma, K. I., and Miyata, T.: MAFFT: a novel method for rapid multiple sequence alignment based on fast Fourier transform, *Nucleic Acids Res.*, 30, 3059–3066, doi: [10.1093/nar/gkf436](https://doi.org/10.1093/nar/gkf436), 2002.
- Kearse, M., Moir, R., Wilson, A., Stones-Havas, S., Cheung, M., Sturrock, S., Buxton, S., Cooper, A., Markowitz, S., Duran, C., Thierer, T., Ashton, B., Mentjies, P., and Drummond, A.: Geneious Basic: an integrated and extendable desktop software platform for the organization and analysis of sequence data, *Bioinformatics*, 28, 1647–1649, doi: [10.1093/bioinformatics/bts199](https://doi.org/10.1093/bioinformatics/bts199), 2012.
- Kekkonen, M., and Hebert, P. D. N.: DNA barcode-based delineation of putative species: Efficient start for taxonomic workflows, *Mol. Ecol. Resour.*, 14, 706–715, doi: [10.1111/1755-0998.12233](https://doi.org/10.1111/1755-0998.12233), 2014.
- Khodami, S., Martinez Arbizu, P., Stöhr, S., and Laakmann, S.: Molecular species delimitation of Icelandic brittle stars (Ophiuroidea), *Pol. Polar Res.*, 35, 243–260, doi: [10.2478/popore-2014-0011](https://doi.org/10.2478/popore-2014-0011), 2014.
- Laakman S., Boos, K., Knebelberger, T., Raupach, M. J., and Neumann, H.: Species identification of echinoderms from the North Sea by combining morphology and molecular data, *Helgol. Mar. Res.* 70, 18, doi: [10.1186/s10152-016-0468-5](https://doi.org/10.1186/s10152-016-0468-5), 2016.
- Layton, K. K. S., Corstorphine, E. A., and Hebert, P. D. N.: Exploring Canadian echinoderm diversity through DNA barcodes, *PLoS ONE* 11, e0166118, doi: [10.1371/journal.pone.0166118](https://doi.org/10.1371/journal.pone.0166118), 2016.
- Legendre, P., and Gallagher, E. D.: Ecologically meaningful transformations for ordination of species data, *Oecologia*, 129, 271–280, doi: [10.1007/s004420100716](https://doi.org/10.1007/s004420100716), 2001.
- Lodge, M., Johnson, D., Le Gurun, G., Wengler, M., Weaver, P., and Gunn, V.: Seabed mining: International Seabed Authority environmental management plan for the Clarion–Clipperton Zone. A partnership approach, *Mar. Policy*, 49, 66–72, doi: [10.1016/j.marpol.2014.04.006](https://doi.org/10.1016/j.marpol.2014.04.006), 2014.
- Ludwig, H.: Die Ophiuren der Sammlung Plate. *Zool. Jahrb. Suppl.* 4, 750–786, 1898.
- Ludwig, H.: Ophiuroideen, in: *Ergebnisse der Hamburger Magalhaensischen Sammelreise 1892/93, I Band*, L. Friedericsen & Co, Hamburg, Germany, 1899.
- Lusty, P. A. J., and Murton, B. J.: Deep-ocean mineral deposits: Metal resources and windows into earth processes, *Elements*, 14, 301–306, doi: [10.2138/gselements.14.5.301](https://doi.org/10.2138/gselements.14.5.301), 2018.
- Lyman, T.: Ophiuridae and Astrophytidae of the exploring voyage of H.M.S. Challenger, under Prof. Sir Wyville Thomson, *F.R.S. Part 1, Bull. Mus. Comp. Zool.*, 5, 65–168, 1878.
- Lyman, T.: Ophiuridae and Astrophytidae of the exploring voyage of H.M.S. Challenger under Prof. Sir Wyville Thomson, *F.R.S. Part 2, Bull. Mus. Comp. Zool.*, 6, 17–83, 1879.

- Lyman, T.: Report on the Ophiuroidea, in: Report on the Scientific Results of the Voyage of H.M.S. Challenger, Zoology, 5,  
605 edited by: Thomson C. W., and Murray, J., H. M. Stationery Off, London, United Kingdom, 1–192, 1882.
- Mero, J. L.: Chapter 11. Economic aspects of nodule mining, in: The mineral resources of the sea, edited by: Mero, J. L.,  
Elsevier, Amsterdam, the Netherlands, 327–355, 1965.
- Miller, K. A., Thompson, K. F., Johnston, P., and Santillo, D.: An overview of seabed mining including the current state of  
development, environmental impacts, and knowledge gaps, *Front. Mar. Sci.*, 4, 418, doi: [10.3389/fmars.2017.00418](https://doi.org/10.3389/fmars.2017.00418), 2018.
- 610 Mukhopadhyay, R., Ghosh, A. K., and Iyer, S. D.: The Indian Ocean nodule field: Geology and resource potential, in:  
Handbook of exploration and environmental geochemistry, volume 10, edited by: Hale, M., Elsevier, Amsterdam, the  
Netherlands, 1–292, 2008.
- Murray, J., and Renard, A. F.: Report on deep-sea deposits based on the specimens collected during the voyage of H.M.S.  
Challenger in the years 1872 to 1876, in: Report on the scientific results of the voyage of H.M.S., Challenger during the years  
615 1873–76, edited by: Thomson C. W., and Murray, J., H. M., Stationery Off, London, United Kingdom, 1–688, 1891.
- Niner, H. J., Ardron, J. A., Escobar, E. G., Gianni, M., Jaeckel, A., Jones, D. O. B., Levin, L. A., Smith, C. R., Thiele, T.,  
Turner, P. J., Van Dover, C.L., Watling, L., and Gjerde, K. M.: Deep-sea mining with no net loss of biodiversity—An impossible  
aim, *Front. Mar. Sci.*, 5, 53, doi: [10.3389/fmars.2018.00053](https://doi.org/10.3389/fmars.2018.00053), 2018.
- Nguyen, L.-T., Schmidt, H. A., von Haeseler, A., and Minh B.Q.: IQ-TREE: A fast and effective stochastic algorithm for  
620 estimating maximum likelihood phylogenies, *Mol. Biol. Evol.*, 32, 268–274, doi: [10.1093/molbev/msu300](https://doi.org/10.1093/molbev/msu300), 2015.
- O'Hara, T.D., Hugall, A. F., Thuy, B., and Moussalli, A.: Phylogenomic resolution of the class Ophiuroidea unlocks a global  
microfossil record, *Curr. Biol.* 24, 1874–1879, doi: [10.1016/j.cub.2014.06.060](https://doi.org/10.1016/j.cub.2014.06.060), 2014.
- O'Hara, T. D., Hugall, A. F., Thuy, B., Stöhr, S., and Martynov, A. V.: Restructuring higher taxonomy using broad-scale  
phylogenomics: the living Ophiuroidea, *Mol. Phylogenet. Evol.*, 107, 415–430, doi: [10.1016/j.ympev.2016.12.006](https://doi.org/10.1016/j.ympev.2016.12.006), 2017.
- 625 Oksanen, J, Kindt, R., Legendre, P., O'Hara, B., Simpson, G. L., Solymos, P., Stevens, M. H. H., and Wagner, H.: The vegan  
Package, *Community ecology package*, 10, 631–637, 2008.
- Puillandre, N., Lambert, A., Brouillet, S., and Achaz, G.: ABGD, Automatic Barcode Gap Discovery for primary species  
Delimitation, *Mol. Ecol.*, 21, 1864–1877, doi: [10.1111/j.1365-294X.2011.05239.x](https://doi.org/10.1111/j.1365-294X.2011.05239.x), 2012.
- Pons, J., Barraclough, T. G., Gomez-Zurita, J., Cardoso, A., Duran, D. P., Hazell, S., Kamoun, S., Sumlin, W. D., and Vogler,  
630 A. P.: Sequence-based species delimitation for the DNA taxonomy of undescribed insects, *Syst. Biol.*, 55, 595–609, doi:  
[10.1080/10635150600852011](https://doi.org/10.1080/10635150600852011), 2006.
- Ramirez-Llodra, E., Brandt, A., Danovaro, R., De Mol, B., Escobar, E., German, C. R., Levin, L. A., Martinez Arbizu, P.,  
Menot, L., Buhl-Mortensen, P., Narayanaswamy, B. E., Smith, C. R., Tittensor, D. P., Tyler, P. A., Vanreusel, A., and  
Vecchione, M.: Deep, diverse and definitely different: unique attributes of the world's largest ecosystem, *Biogeosciences*, 7,  
635 2851–2899, doi: <https://doi.org/10.5194/bg-7-2851-2010>, 2010.

- Ramirez-Llodra, E., Tyler, P. A., Baker, M. C., Bergstad, O. A., Clark, M. R., Escobar, E., Levin, L. A., Menot, L., Rowden, A. A., Smith, C. R., and Van Dover, C. L.: Man and the Last Great Wilderness: Human Impact on the Deep Sea, *PLoS ONE* 6, e22588, doi: [10.1371/journal.pone.0022588](https://doi.org/10.1371/journal.pone.0022588), 2011.
- Ratnasingham, S., and Hebert, P. D. N.: A DNA-based registry for all animal species: The barcode index number (BIN) system. *PLoS ONE*, 8, e66213, doi: [10.1371/journal.pone.0066213](https://doi.org/10.1371/journal.pone.0066213), 2013.
- Rex, M. A., and Etter, R.J.: *Deep-Sea Biodiversity: Pattern and Scale*, Harvard University Press, Cambridge, U.S.A., 2010.
- Simpson, G. G.: Mammals and the nature of continents, *Am. J. Sci.*, 241, 1–31, 1943.
- Smith, A. B., Paterson G. L. J., and Lafay B.: Ophiuroid phylogeny and higher taxonomy: morphological, molecular and palaeontological perspectives, *Zool. J. Linnean Soc.*, 114, 213–243, 1995.
- 645 Smith, C. R., De Leo, F. C., Bernardino, A. F., Sweetman, A. K., and Martinez Arbizu, P.: Abyssal food limitation, ecosystem structure and climate change, *Trends Ecol. Evolut.*, 23, 518–528, doi: [10.1016/j.tree.2008.05.002](https://doi.org/10.1016/j.tree.2008.05.002), 2008.
- Song, C., Lin, X.-L., Wang, Q., and Wang, X.-H.: DNA barcodes successfully delimit morphospecies in a superdiverse insect genus, *Zool. Scr.*, 00, 1–14, doi: [10.1111/zsc.12284](https://doi.org/10.1111/zsc.12284), 2018.
- Sørensen, T.: A method of establishing groups of equal amplitude in plant sociology based on similarity of species content and its application to analyses of the vegetation on Danish commons, *Biol. Skr. Dan. Vid. Sel.*, 5, 1–34, 1948.
- 650 Stöhr, S., O'Hara, T. D., and Thuy, B.: Global Diversity of Brittle Stars (Echinodermata: Ophiuroidea), *PLoS ONE*, 7, e31940, doi: [10.1371/journal.pone.0031940](https://doi.org/10.1371/journal.pone.0031940), 2012.
- Stratmann, T., Lins, L., Purser, A., Marcon, Y., Rodrigues, C. F., Ravara, A., Cunha, M. R., Simon-Lledó, E., Jones, D. O. B., Sweetman, A. K., Köser, K., and van Oevelen, D.: Abyssal plain faunal carbon flows remain depressed 26 years after a simulated deep-sea mining disturbance, *Biogeosciences*, 15, 4131–4145, doi: [10.5194/bg-15-4131-2018](https://doi.org/10.5194/bg-15-4131-2018), 2018.
- 655 Taboada, S., Riesgo, A., Wiklund, H., Paterson, G. L. J., Koutsouveli, V., Santodomingo, N., Dale, A. C., Smith, C. R., Jones, D. O. B., Dahlgren, T. G., and Glover, A. G.: Implications of population connectivity studies for the design of marine protected areas in the deep sea: An example of a demosponge from the Clarion-Clipperton Zone, *Mol. Ecol.*, 27, 4657–4679, doi: [10.1111/mec.14888](https://doi.org/10.1111/mec.14888), 2018.
- 660 Tang, C. Q., Humphreys, A. M., Fontaneto, D., Barraclough, T. G., and Paradis, E.: Effects of phylogenetic reconstruction method on the robustness of species delimitation using single-locus data, *Methods Ecol. Evol.*, 5, 1086–1094, doi: [10.1111/2041-210X.12246](https://doi.org/10.1111/2041-210X.12246), 2014.
- Thiel, H., and Schriever, G.: *Deep-Sea Mining, Environmental Impact and the DISCOL Project*, *Ambio*, 19, 245–250, 1990.
- Thiel, H., Schriever, G., Ahnert, A., Bluhm, H., Borowski, C., and Vopel, K.: The large-scale environmental impact experiment DISCOL: reflection and foresight, *Deep-Sea Res. II*, 48, 3869–3882, doi: [10.1016/S0967-0645\(01\)00071-6](https://doi.org/10.1016/S0967-0645(01)00071-6), 2001..
- 665 Tilot, V., Ormond, R., Moreno Navas, J., and Catalá T. S.: The Benthic Megafaunal Assemblages of the CCZ (Eastern Pacific) and an Approach to their Management in the Face of Threatened Anthropogenic Impacts, *Front. Mar. Sci.*, 5, doi: [10.3389/fmars.2018.00007](https://doi.org/10.3389/fmars.2018.00007), 2018.

- Van Dover, C. L., Ardron, J. A., Escobar, E., Gianni, M., Gjerde, K. M., Jaeckel, A., Jones, D. O. B., Levin, L. A., Niner, H. J., Pendleton, L., Smith, C. R., Thiele, T., Turner, P. J., Watling, L., and Weaver, P. P. E.: Biodiversity loss from deep-sea mining, *Nat. Geosci.*, 10, 464, doi: 10.1038/ngeo2983, 2017.
- Vanreusel, A., Hilario, A., Ribeiro, P. A., Menot, L., and Arbizu, P. M.: Threatened by mining, polymetallic nodules are required to preserve abyssal epifauna, *Sci. Rep.*, 6, 26808, doi: 10.1038/srep26808, 2016.
- Volz, J. B., Mogollon, J. M., Geibert, W., Arbizu, P. M., Koschinsky, A., and Kasten, S.: Natural spatial variability of depositional conditions, biogeochemical processes and element fluxes in sediments of the eastern Clarion-Clipperton Zone, Pacific Ocean, *Deep Sea Res. Part I Oceanogr. Res. Pap.*, 140, 159-172, doi: 10.1016/j.dsr.2018.08.006, 2018.
- Volz, J. B., Haffert L., Haeckel M., Koschinsky, A., Kasten, S.: Impact of small-scale disturbances on geochemical conditions, biogeochemical processes and element fluxes in surface sediments of the eastern Clarion-Clipperton Zone, Pacific Ocean. *Biogeosciences Discuss*, doi: 10.5194/bg-2019-316, in review, 2019.
- Wedding, L. M., Friedlander, A. M., Kittinger, J. N., Watling, L., Gaines, S. D., Bennett, M., Hardy, S. M., and Smith, C. R.: From principles to practice: a spatial approach to systematic conservation planning in the deep sea, *Proc. R. Soc. Lond. Biol.*, 280, 1684–1684, doi: [10.1098/rspb.2013.1684](https://doi.org/10.1098/rspb.2013.1684), 2013.
- Zhang, J., Kapli, P., Pavlidis, P., and Stamatakis, A.: A general species delimitation method with applications to phylogenetic placements, *Bionformatics*, 29, 2869–2876, doi: [10.1093/bioinformatics/btt499](https://doi.org/10.1093/bioinformatics/btt499), 2013.

685

## Tables

**Table 1.** Mean genetic distance values (p-distance) and range of intraspecific distances for the ophiuroid species. N indicating the number of sampled individuals followed by H, the number of unique haplotypes, and values following the mean genetic distance represent standard deviations.

690

No.	Species	Family	N	H	Mean	Range
Species 1	<i>Ophiotholia</i> sp.	Ophiohelidae	20	19	0.013±0.00384	0.000–0.024
Species 2	<i>Amphioplus daleus</i>	Amphiuridae	36	31	0.006±0.00382	0.000–0.021
Species 3	<i>Ophiosphalma glabrum</i>	Ophiosphalmidae	34	28	0.009±0.00392	0.000–0.021
Species 4	<i>Amphioplus</i> cf. <i>daleus</i>	Amphiuridae	2	2	0.055	--
Species 5	<i>Amphilepis</i> sp.	Amphilepididae	6	6	0.016±0.00675	0.005–0.024
Species 6	<i>Ophiuroglypha</i> cf. <i>polyacantha</i>	Ophiuridae	10	9	0.004±0.00215	0.000–0.008
Species 7	<i>Ophiuroglypha</i> sp.	Ophiuridae	1	1	--	--
Species 8	Ophiopyrgidae sp.	Ophiopyrgidae	1	1	--	--
Species 9	<i>Ophiuroglypha</i> sp.	Ophiuridae	14	14	0.009±0.00375	0.002–0.018

Species 10	<i>Anophiura</i> sp.	Ophiopyrgidae	1	1	--	--
Species 11	<i>Ophiuroglypha</i> sp.	Ophiuridae	1	1	--	--
Species 12	<i>Asteroschema</i> sp.	Euryalidae	1	1	--	--
Species 13	<i>Perlophiura profundissima</i>	Ophiosphalmidae	2	2	0.003	--
Species 14	<i>Ophiuroglypha</i> sp.	Ophiuridae	1	1	--	--
Species 15	<i>Ophiophyllum</i> sp.	Ophiopyrgidae	2	1	0.000	--
Species 16	<i>Amphiophiura bullata</i>	Ophiopyrgidae	11	11	0.006±0.00316	0.002–0.014
Species 17	Ophioscolecidae sp.	Ophioscolecidae	3	1	0.000	0.000–0.000
Species 18	Ophioscolecidae sp.	Ophioscolecidae	3	3	0.012±0.00643	0.005–0.017
Species 19	Ophioscolecidae sp.	Ophioscolecidae	1	1	--	--
Species 20	Ophioscolecidae sp.	Ophioscolecidae	4	2	0.003±0.00329	0.000–0.006
Species 21	<i>Ophiotoma</i> sp.	Ophioscolecidae	3	2	0.002±0.00173	0.000–0.003
Species 22	Ophioleucidae sp.	Ophioleucidae	4	4	0.005±0.00117	0.003–0.006
Species 23	<i>Ophioleuce gracilis</i>	Ophioleucidae	1	1	--	--
Species 24	<i>Ophiocymbium</i> sp.	Ophioscolecidae	7	3	0.010±0.00992	0.000–0.021
Species 25	<i>Ophiocymbium</i> sp.	Ophioscolecidae	2	2	0.028	--
Species 26	<i>Ophiomyces</i> sp.	Ophiohelidae	8	8	0.005±0.00179	0.002–0.008
Species 27	<i>Ophiacantha cosmica</i>	Ophiacanthidae	19	11	0.003±0.00212	0.000–0.009
Species 28	<i>Ophiotholia</i> sp.	Ophiohelidae	7	5	0.031±0.02874	0.000–0.076
Species 29	Ophioleucidae sp.	Ophioleucidae	28	12	0.004±0.00555	0.000–0.002
Species 30	<i>Ophiotypa simplex</i>	Ophiolepididae	6	5	0.004±0.00234	0.000–0.009
Species 31	<i>Ophiernus</i> sp.	Ophiernidae	4	3	0.019±0.00501	0.002–0.024
Species 32	Ophiohelidae sp.	Ophiohelidae	1	1	--	--
Species 33	Ophioleucidae sp.	Ophioleucidae	1	1	--	--
Species 34	Ophioleucidae sp.	Ophioleucidae	1	1	--	--
Species 35	Ophioleucidae sp.	Ophioleucidae	10	5	0.002±0.00172	0.000–0.005
Species 36	<i>Ophiosphalma</i> cf. <i>glabrum</i>	Ophiosphalmidae	22	21	0.012±0.00426	0.000–0.024
Species 37	Ophioleucidae sp.	Ophioleucidae	5	4	0.007±0.00405	0.000–0.014
Species 38	Ophioscolecidae sp.	Ophioscolecidae	4	3	0.004±0.00245	0.000–0.006
Species 39	<i>Ophiocymbium</i> sp.	Ophioscolecidae	2	2	0.011	--
Species 40	<i>Ophiocymbium</i> sp.	Ophioscolecidae	6	5	0.026±0.01113	0.000–0.040
Species 41	<i>Ophiotholia</i> sp.	Ophiohelidae	1	1	--	--

Species 42	Ophioleucidae sp.	Ophioleucidae	1	1	--	--
Species 43	<i>Ophiuroglypha</i> cf. <i>polyacantha</i>	Ophiuridae	4	3	0.004±0.00205	0.000–0.008

---

**Table 2:** Species composition table showing the number of specimens from each species found adding up all samples for a given area.

Species		UKSRL	BGR	IFREMER	GSR	IOM	APEI3	DISCOL
<i>Ophiotholia</i> _sp1	Species 1	16	28	0	0	0	0	0
<i>Amphioplus daleus</i> _sp2	Species 2	64	95	8	5	15	0	19
<i>Ophiosphalma glabrum</i> _sp3	Species 3	12	27	1	13	11	0	1
<i>Amphioplus</i> cf. <i>daleus</i> _sp4	Species 4	2	0	0	0	0	0	0
<i>Amphilepis</i> _sp5	Species 5	0	4	0	0	0	0	2
<i>Ophiuroglypha</i> cf. <i>polyacantha</i> _sp6	Species 6	5	4	0	0	0	0	1
<i>Ophiuroglypha</i> _sp7	Species 7	0	0	0	0	0	0	1
Ophiopyrgidae_sp8	Species 8	0	1	0	0	0	0	0
<i>Ophiuroglypha</i> _sp9	Species 9	0	0	0	0	0	14	0
<i>Anophiura</i> _sp10	Species 10	0	1	0	0	0	0	0
<i>Ophiuroglypha</i> _sp11	Species 11	0	1	0	0	0	0	0
<i>Asteroschema</i> _sp12	Species 12	0	0	0	0	0	1	0
<i>Perlophiura profundissima</i> _sp13	Species 13	1	0	0	0	0	0	4
<i>Ophiuroglypha</i> _sp14	Species 14	0	1	0	0	0	0	0
<i>Ophiophyllum</i> _sp15	Species 15	0	0	0	1	0	1	0
<i>Amphiophiura bullata</i> _sp16	Species 16	2	1	1	7	0	0	0
Ophioscolecidae_sp17	Species 17	0	0	0	0	0	3	0
Ophioscolecidae_sp18	Species 18	0	2	0	0	0	0	1
Ophioscolecidae_sp19	Species 19	1	0	0	0	0	0	0
Ophioscolecidae_sp20	Species 20	0	0	1	0	0	3	0
<i>Ophiotoma</i> _sp21	Species 21	0	1	0	0	0	0	2
Ophioleucidae_sp22	Species 22	1	3	0	0	0	0	0
<i>Ophioleuce gracilis</i> _sp23	Species 23	0	1	0	0	0	0	0
<i>Ophiocymbium</i> _sp24	Species 24	5	0	0	0	0	2	0
<i>Ophiocymbium</i> _sp25	Species 25	2	0	0	0	0	0	0
<i>Ophiomyces</i> _sp26	Species 26	8	0	0	0	0	0	0
<i>Ophiacantha cosmica</i> _sp27	Species 27	1	16	0	1	0	0	2
<i>Ophiotholia</i> _sp28	Species 28	5	1	0	0	0	1	0
Ophioleucidae_sp29	Species 29	5	10	2	3	4	0	4
<i>Ophiotypa simplex</i> _sp30	Species 30	3	1	0	1	1	0	0
<i>Ophiernus</i> _sp31	Species 31	0	1	0	0	0	0	3

Ophioidae_sp32	Species 32	0	0	0	0	0	1	0
Ophioidae_sp33	Species 33	1	0	0	0	0	0	0
Ophioidae_sp34	Species 34	0	1	0	0	0	0	0
Ophioidae_sp35	Species 35	2	3	0	3	2	0	0
<i>Ophioidae cf. glabrum</i> _sp36	Species 36	19	11	0	1	0	0	4
Ophioidae_sp37	Species 37	0	0	0	1	0	4	0
Ophioidae_sp38	Species 38	0	0	0	0	0	0	4
<i>Ophioidae</i> _sp39	Species 39	1	1	0	0	0	0	0
<i>Ophioidae</i> _sp40	Species 40	1	4	0	0	0	0	1
<i>Ophioidae</i> _sp41	Species 41	0	0	0	0	1	0	0
Ophioidae_sp42	Species 42	0	0	0	0	0	1	0
<i>Ophioidae cf. polyacantha</i> _sp43	Species 43	1	0	0	2	1	0	0

---

**Table 3.** Summary of diversity parameters per sampled area. Sites = number of collection sites, N = number of specimens, S = number of Species, Usp = number of unique species, Chao ± SE = Chao estimated number of species with standard error, ACE ± SE = ACE estimated number of species with standard error, H' = Shannon Diversity, 1-D = Simpson Diversity and J = Jaccard's Evenness.  $\beta_{SOR}$ ,  $\beta_{SIM}$  and  $\beta_{SNE}$  express multiple-site total beta diversity, multiple-site species turnover and multiple-site nestedness respectively. Note that in the rows of each area the value is the result of excluding this area, except for the row Total, which includes all areas.

AREA	Sites	N	S	Usp	Chao±SE	ACE±SE	H'	1-D	J	$\beta_{SOR}$	$\beta_{SIM}$	$\beta_{SNE}$
UKSRL	5	158	22	5	27.2±5.3	30.5±2.7	2.18	0.79	0.70	0.786	0.656	0.130
BGR	18	219	24	6	57±26.3	51.1±4.9	2.04	0.76	0.64	0.784	0.663	0.121
IFREMER	4	13	5	0	6.5±2.5	12±1.8	1.17	0.57	0.73	0.756	0.634	0.122
GSR	5	38	11	0	16±5.9	17.1±2	1.97	0.81	0.82	0.782	0.635	0.146
IOM	3	35	7	1	8.5±2.5	11.5±1.5	1.44	0.69	0.74	0.759	0.620	0.138
APEI3	6	31	10	5	15±5.9	15.2±1.8	1.80	0.75	0.78	0.717	0.488	0.229
DISCOL	14	49	14	2	16.5±3.1	17±1.8	2.14	0.81	0.81	0.771	0.604	0.167
<b>Total</b>	<b>55</b>	<b>543</b>	<b>43</b>	-	<b>57</b>	<b>53.5</b>	<b>2.50</b>	<b>0.82</b>	<b>0.66</b>	<b>0.782</b>	<b>0.640</b>	<b>0.142</b>

**Table 4.** Faunistic similarity between areas. Upper diagonal = number of shared species, lower diagonal = number of unshared species. Bold numbers indicate the number of species in each area.

	UKSRL	BGR	IFREMER	GSR	IOM	APEI3	DISCOL
UKSRL	0\22	14	4	9	6	2	8
BGR	18	0\24	4	8	5	1	11
IFREMER	19	21	0\5	4	3	1	3
GSR	15	19	8	0\11	6	2	5
IOM	17	21	6	6	0\7	0	3
APEI3	28	32	13	17	17	0\10	0
DISCOL	20	16	13	13	15	24	0\14

## Figure Legends

**Figure 1.** Compilation of study areas in the Clarion-Clipperton Fracture Zone (CCZ) and in the DISCOL Experimental Area (DEA, Peru Basin). Insets represent detailed maps of sampling locations in the IFREMER, GSR, IOM, BGR, UKSRL exploration license areas for polymetallic nodules as well as in APEI3 (ISA protected area) and the DEA.

**Figure 2.** Neighbour-Joining tree (p-distance) based on 300 brittle star COI DNA barcodes. Black circles on branches represent bootstrap supports  $\geq 90\%$ . The results of species delimitation analyses, (ABGD, BINs, st-GMYC, and mPTP) are shown on the right-hand margin of the tree.

**Figure 3.** Maximum Likelihood phylogenetic tree based on 300 brittle star COI DNA barcodes calculated using IQ-tree. Black circles on branches represent bootstrap support ( $\geq 90\%$ ).

**Figure 4.** Histogram showing the percentage of genetic p-distances within and between brittle star species based on the 657bp "barcode" fragment of COI gene. Intraspecific and interspecific variations are shown in yellow and interspecific variation shown in red and yellow respectively.

**Figure 5.** *Amphilepis* sp. (sp5): **A**, dorsal and ventral view, MA13\_85\_32; **B**, dorsal and ventral view, MA14\_39\_9. *Amphioplus (Unioplus) daleus* (sp2): **C**, dorsal and ventral view, AB2\_EB1\_16\_13; **D**, dorsal and ventral view, AB1\_EB5\_10\_4; **E**, dorsal and ventral view, SO239\_81\_07. Scale bars: 0.5 mm (A, C–D); 1 mm (B); 2 mm (E).

**Figure 6.** *Amphioplus (Unioplus) daleus* (sp2): **A**, dorsal and ventral view, MA14\_38\_01. *Amphioplus (Unioplus) cf. daleus* (sp4): **B**, dorsal and ventral view, AB2\_EB1\_14\_27. *Ophiernus* sp. (sp31): **C**, dorsal and ventral view of disc and detached arms, MA14\_21\_12. *Ophiotypa simplex* (sp30): **D**, dorsal and ventral view, AB2\_EB2\_12\_3; **E**, dorsal and ventral view, AB1\_EB5\_4. Scale bars: 0.5 mm (A, D); 2 mm (B); 1 mm (C, E).

**Figure 7.** *Ophiotypa simplex* (sp30): **A**, dorsal and ventral view, SO239\_118\_1. *Ophioleuce gracilis* (sp23): **B**, dorsal and ventral view, SO239\_397. Ophioleucidae sp. (sp22): **C**, dorsal and ventral view, SO239\_24\_17; **D**, dorsal and ventral view, SO239\_59\_1. Ophioleucidae sp. (sp29): **E**, dorsal and ventral view, SO239\_24\_12. Scale bars: 2 mm (A, B); 1 mm (D); 0.5 mm (E, C).

**Figure 8.** Ophioleucidae sp. (sp29): **A**, dorsal and ventral view, SO239\_24\_3. Ophioleucidae sp. (sp33): **B**, dorsal and ventral view, AB1\_EB5\_10\_9. Ophioleucidae sp. (sp34): **C**, dorsal and ventral view, MA14\_21\_3. Ophioleucidae sp. (sp35): **D**, dorsal and ventral view, SO239\_118\_14; **E**, dorsal and ventral view, SO239\_24\_5; **F**, dorsal and ventral view, SO239\_133\_2. Scale bars: 1 mm (A, C, E, F); 0.5 mm (B, D).

**Figure 9.** Ophioleucidae sp. (sp37): **A**, dorsal and ventral view, SO239\_139\_2. *Asteroschema* sp. (sp12): **B**, in situ (up left and right), specimen collected with the ROV KIEL 6000 in dorsal (down left) and ventral (down right) view, SO239\_2113. *Ophiocantha cosmica*: **C**, in situ (left), specimen collected with the ROV KIEL 6000 in dorsal view (right), SO239\_130. Scale bars: 2 mm (A); 1 cm (B, C). Copyright (for in situ photos): ROV KIEL 6000 Team/ GEOMAR Kiel.

**Figure 10.** *Ophiocantha cosmica* (sp27): **A**, dorsal and ventral view, MA14\_20\_4; **B**, specimen collected with the ROV KIEL 6000 in dorsal and ventral view (up), in situ (down), SO242-2\_191\_F5. *Ophiotoma* sp. (sp21): **C**, dorsal and ventral view,

SO239\_20\_12. *Ophiocymbium* sp. (sp24): **D**, dorsal and ventral view. *Ophiocymbium* sp. (sp39): **E**, AB2\_EB1\_13\_41; dorsal and ventral view, AB2\_EB1\_13\_8. Scale bars: 0.5 cm (D); 1 mm (A, C); 1 cm (B); 2 mm (E). Copyright (for in situ photos): ROV KIEL 6000 Team/ GEOMAR Kiel.

**Figure 11.** *Ophiocymbium* sp. (sp40): **A**, dorsal and ventral view, SO239\_24\_19; **B**, dorsal and ventral view, MA14\_21\_10. Ophiohelidae sp. (sp32): **C**, dorsal and ventral view, SO239\_192\_06. *Ophiomyces* sp. (sp26): **D**, dorsal and ventral view, AB1\_EB5\_10\_3; **E**, dorsal and ventral view, AB1\_EB4\_11\_24; **F**, lateral view, AB1\_EB4\_11\_22. *Ophiotholia* sp. (sp1): **G**, dorsal and ventral view, MA14\_38\_13. Scale bars: 0.5 mm (A, C); 1 mm (B, E, F); 0.2 mm (D).

**Figure 12.** *Ophiotholia* sp. (sp1): **A**, lateral view, MA13\_85\_3; **B**, lateral view, MA13\_90\_18. *Ophiotholia* sp. (sp28): **C**, dorsal and ventral view, MA14\_66\_10. Ophioscocidae sp. (sp17): **D**, dorsal and ventral view, SO239\_197\_4. Ophioscocidae sp. (sp18): **E**, dorsal and ventral view, SO239\_24\_21. Ophioscocidae sp. (sp19): **F**, dorsal and ventral view, AB2\_EB2\_12\_10. Ophioscocidae sp. (sp20): **G**, dorsal and ventral view, SO239\_192\_2; **H**, dorsal and ventral view, SO239\_192\_8. *Amphiophiura bullata* (sp16): **I**, dorsal and ventral view, SO239\_118\_13. Scale bars: 1 mm (A–D, G, H); 0.5 mm (E–F, I).

**Figure 13.** *Amphiophiura bullata* (sp16): **A**, dorsal view (up) and dorsal (down left) and ventral view (down right) of disc, SO239\_133\_3; **B**, dorsal and ventral view, MA13\_90\_16. *Anophiura* sp. (sp10): **C**, dorsal view and detail dorsal and ventral view of disc, SO239\_396. *Ophiophyllum* sp. (sp15): **D**, dorsal and ventral view, SO239\_139\_1. Ophiopyrgidae sp. (sp8): **E**, dorsal and ventral view, SO239\_59\_10. Scale bars: 0.5 mm (A, D); 2 mm (B); 1 mm (C, E).

**Figure 14.** *Ophiuroglypha* cf. *polyacantha* (sp6): **A**, dorsal and ventral view, MA14\_66\_7; **B**, dorsal and ventral view, SO242-2\_222\_F1. *Ophiuroglypha* cf. *polyacantha* (sp43): **C**, dorsal and ventral view, SO239\_118\_6; **D**, in situ (right), dorsal and ventral view (left), SO239\_2037. *Ophiuroglypha* sp. (sp14): **E**, dorsal and ventral view, SO239\_59\_18. Scale bars: 0.5 mm (A, E); 1 mm (C); 1 cm (B, D). Copyright (for in situ photos): ROV KIEL 6000 Team/ GEOMAR Kiel.

**Figure 15.** *Ophiuroglypha* sp. (sp11): **A**, dorsal and ventral view, SO239\_395. *Ophiuroglypha* sp. (sp7): **B**, dorsal and ventral view, SO242-2\_176\_F8. *Ophiuroglypha* sp. (sp9): **C**, in situ (up right), dorsal and ventral view, detail ventral view of disc (down right), SO239\_2059. *Ophiosphalma glabrum* (sp3): **D**, dorsal and ventral view, AB1\_EB5\_10\_7. Scale bars: 1 cm (A, B–C); 0.5 mm (D). Copyright (for in situ photos): ROV KIEL 6000 Team/ GEOMAR Kiel.

**Figure 16.** *Ophiosphalma glabrum* (sp3): **A**, dorsal and ventral view, SO239\_24\_4; **B**, dorsal and ventral view, SO239\_50\_2; **C**, dorsal and ventral view, SO242-2\_222\_F2. *Ophiosphalma* cf. *glabrum* (sp36): **C**, dorsal and ventral view, SO239\_24\_18; **D**, dorsal and ventral view, AB2\_EB1\_14\_2; **E**, dorsal and ventral view, SO239\_24-1\_1; **F**, dorsal and ventral view, SO239\_2014. *Perlophiura profundissima*: **G**, dorsal and ventral view, SO242-1\_387\_A7. Scale bars: 0.5 mm (C, E) 1 mm (D, B, G); 2 mm (A, E); 1 cm (F).

**Figure 17.** Relationship between number of specimens (N) and number of species (S) in the areas examined

**Figure 18.** Sample-based rarefaction curves of the examined areas. The inset shows a close-up for the minimum shared number of specimens (12).

**Figure 19.** Resulting Beta diversity, when each is excluded from calculation, decomposed into its additive components species turnover (light blue) and nestedness (orange). Excluding APEI3 has the greatest impact on beta diversity. First bar 'Total' shows the values including all areas.

**Figure 20.** nMDS based on Chord distance between areas.

**Figure 21.** Box and Whiskers Plot of the Chord distance of each area to other areas.

**Figure 22.** nMDS based on Euclidean distance on presence/absence data.

**Figure 23.** Box and Whiskers Plot of the Euclidean distance on presence/absence data of each area to other areas.

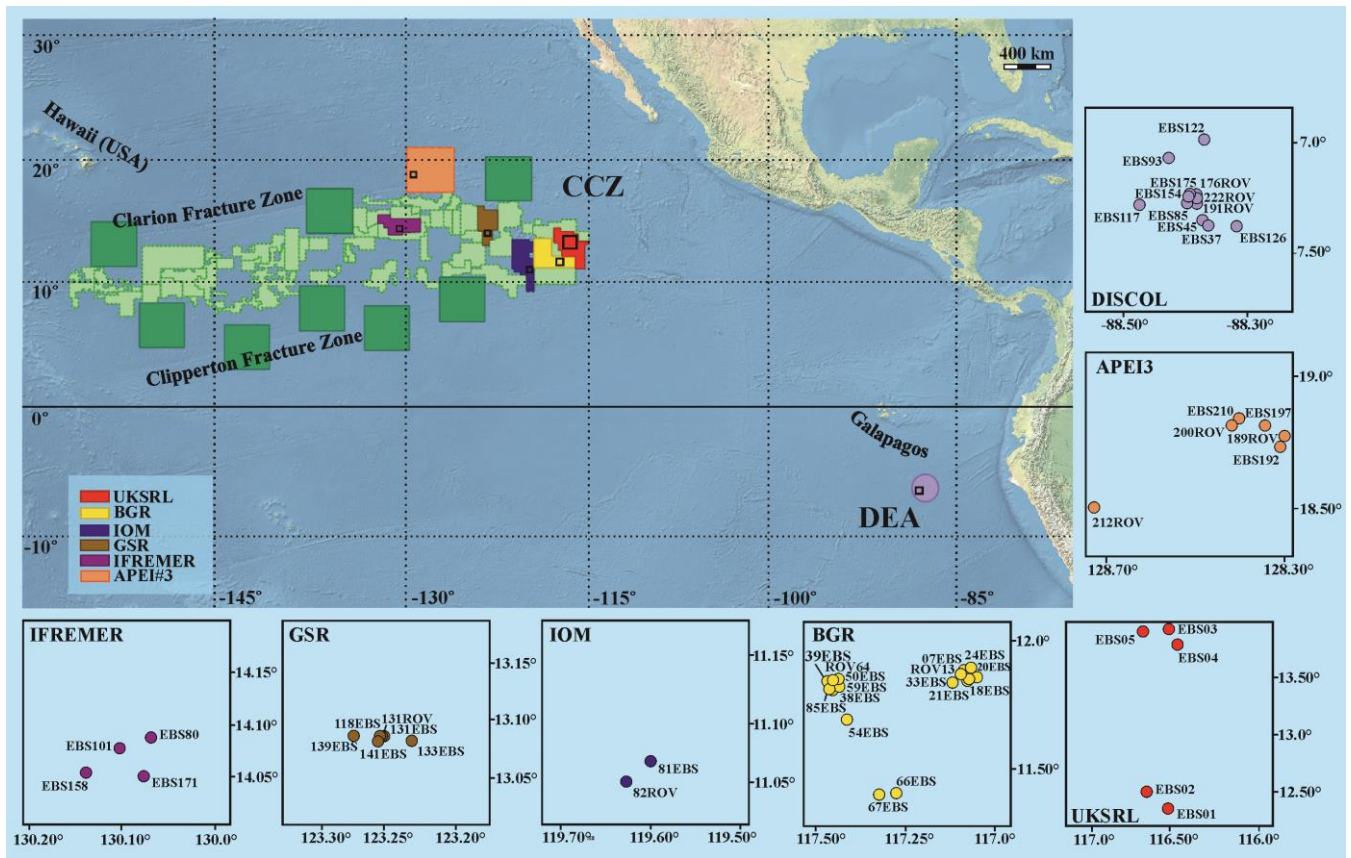


Figure 1



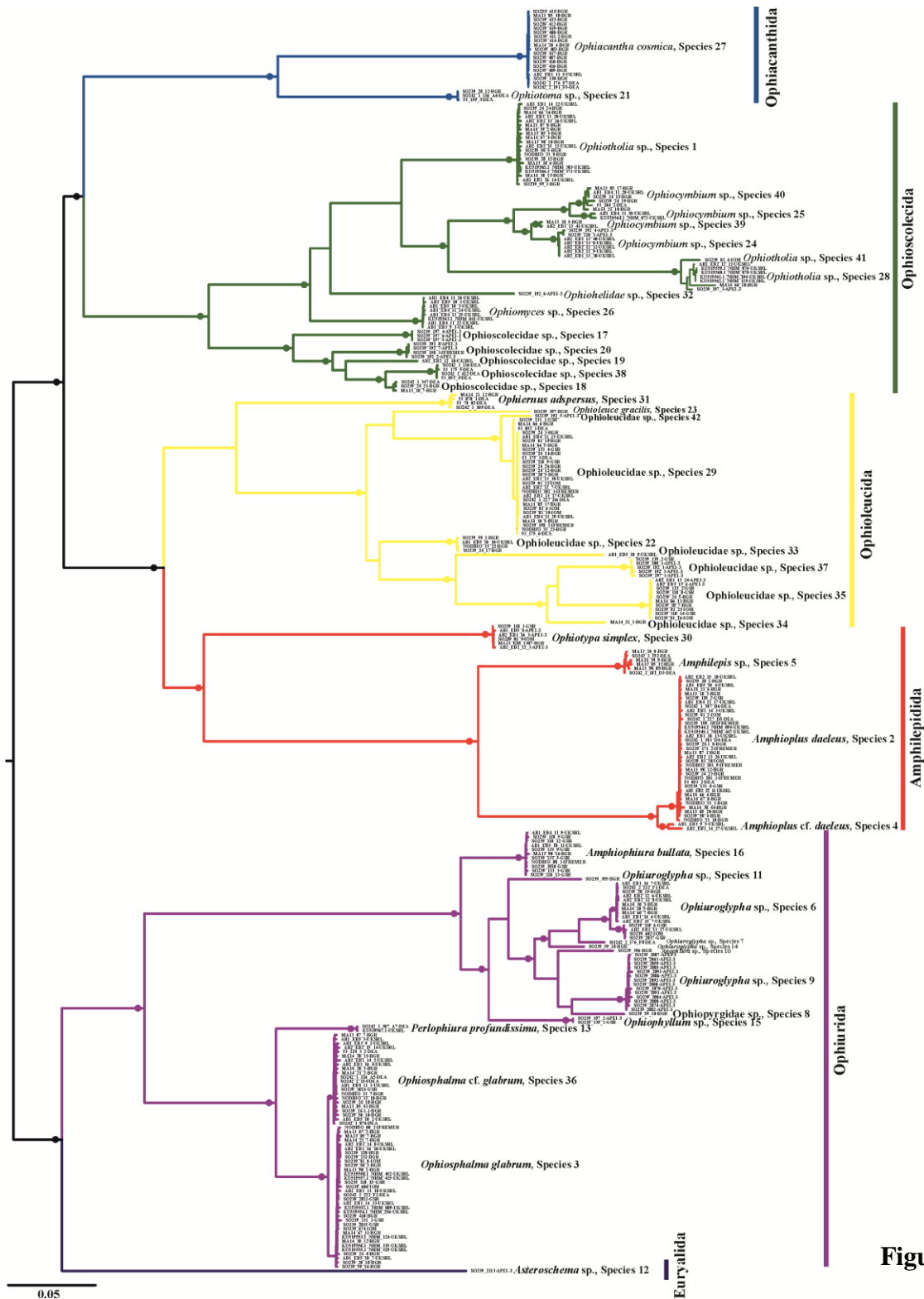


Figure 3

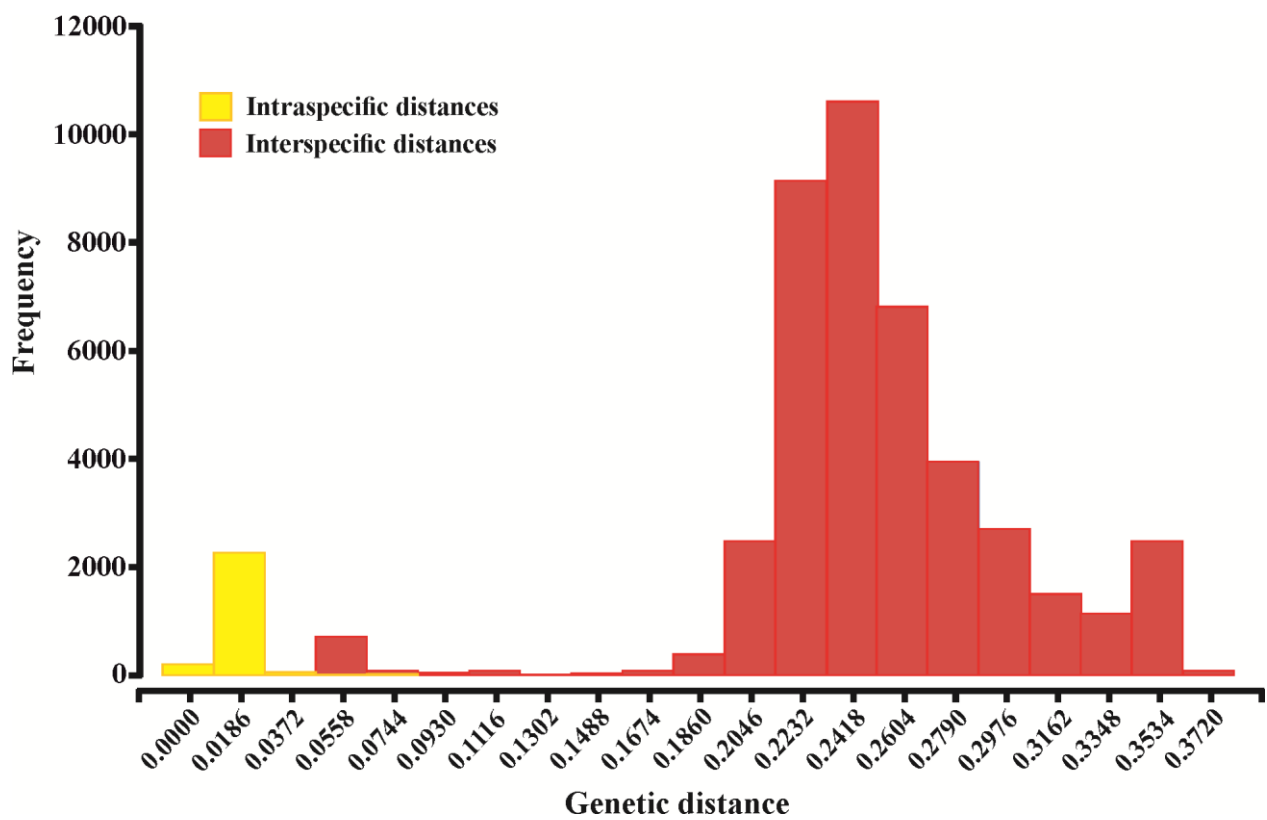
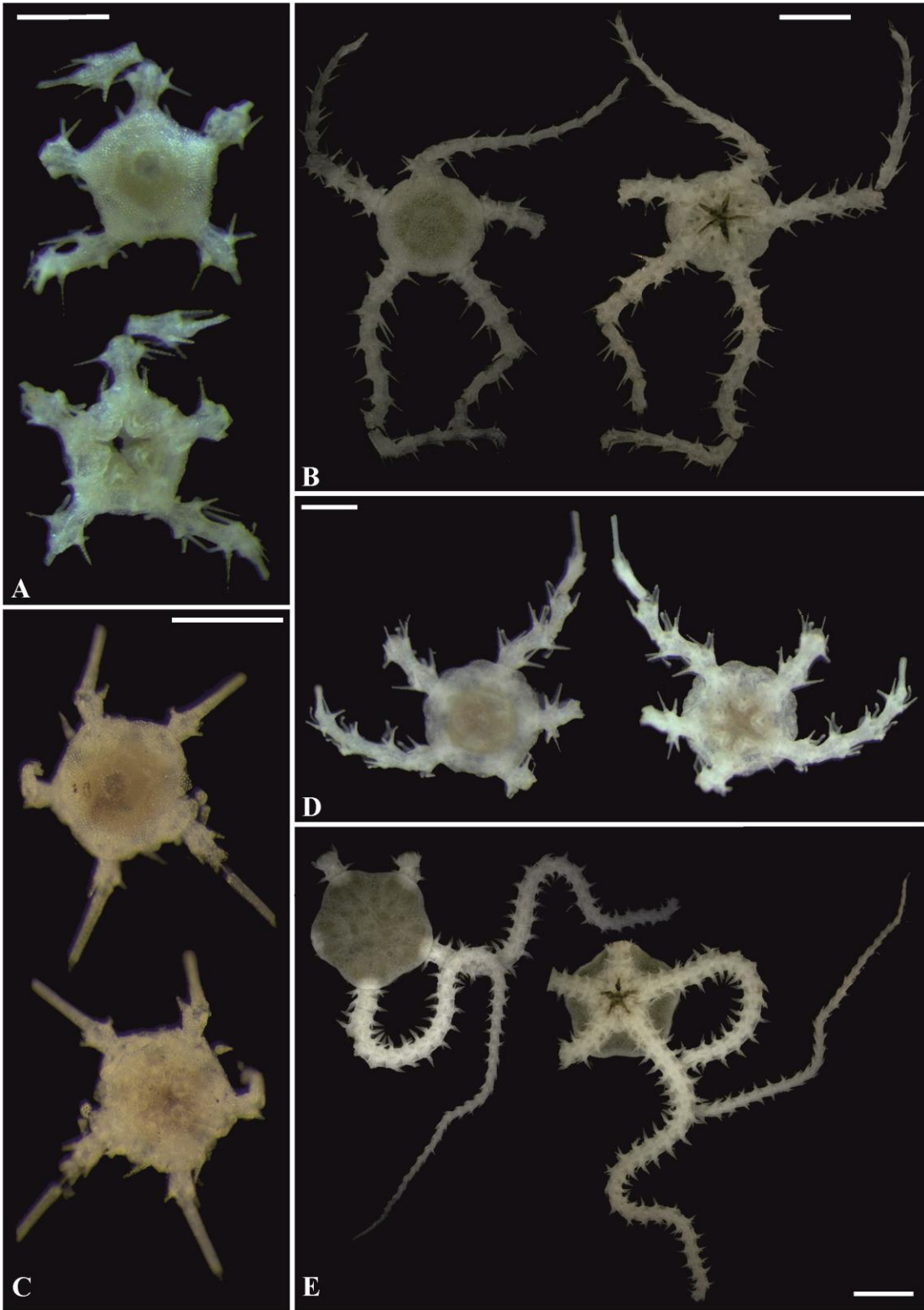
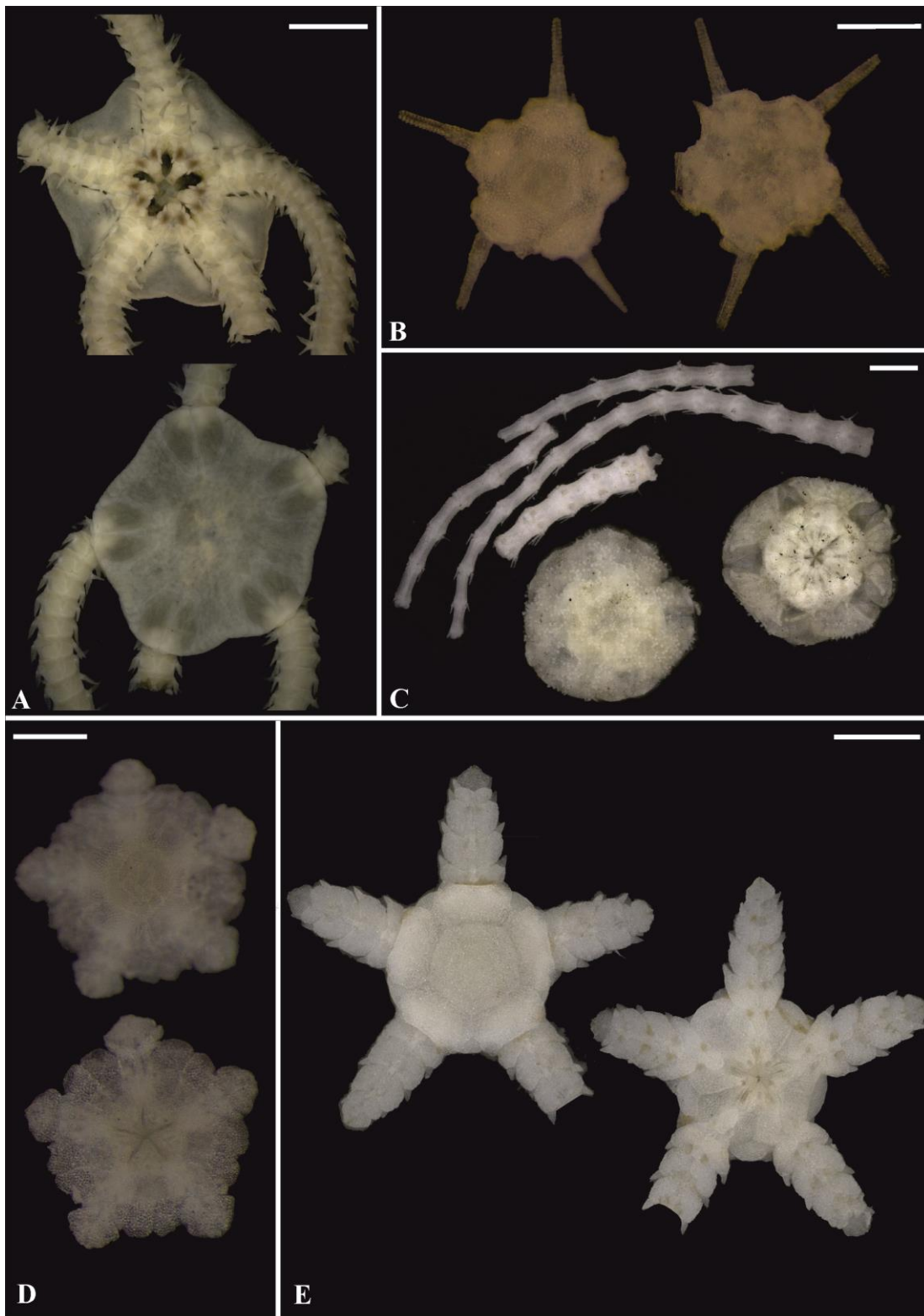


Figure 4



**Figure 5**



**Figure 6**

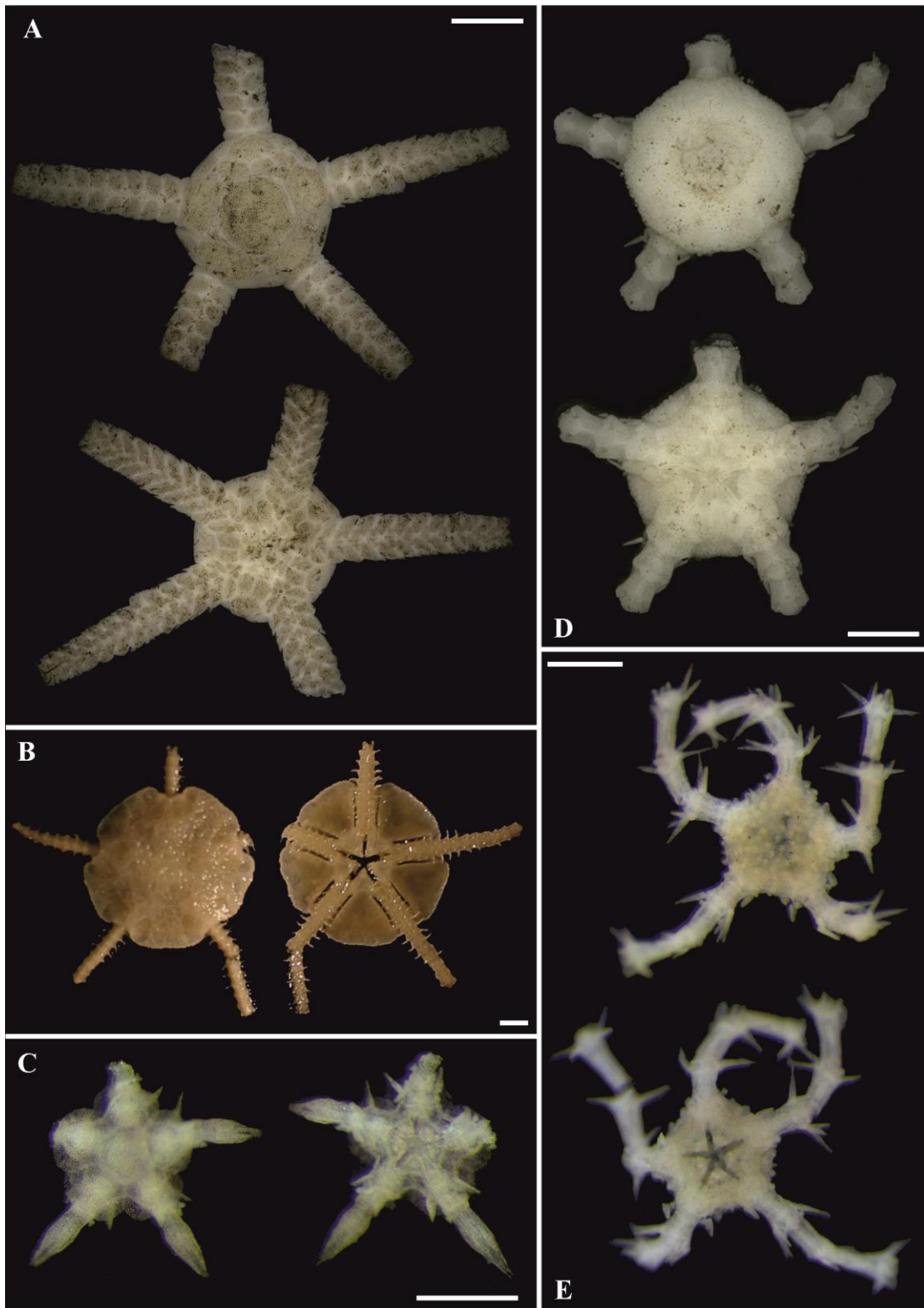


**Figure 7**

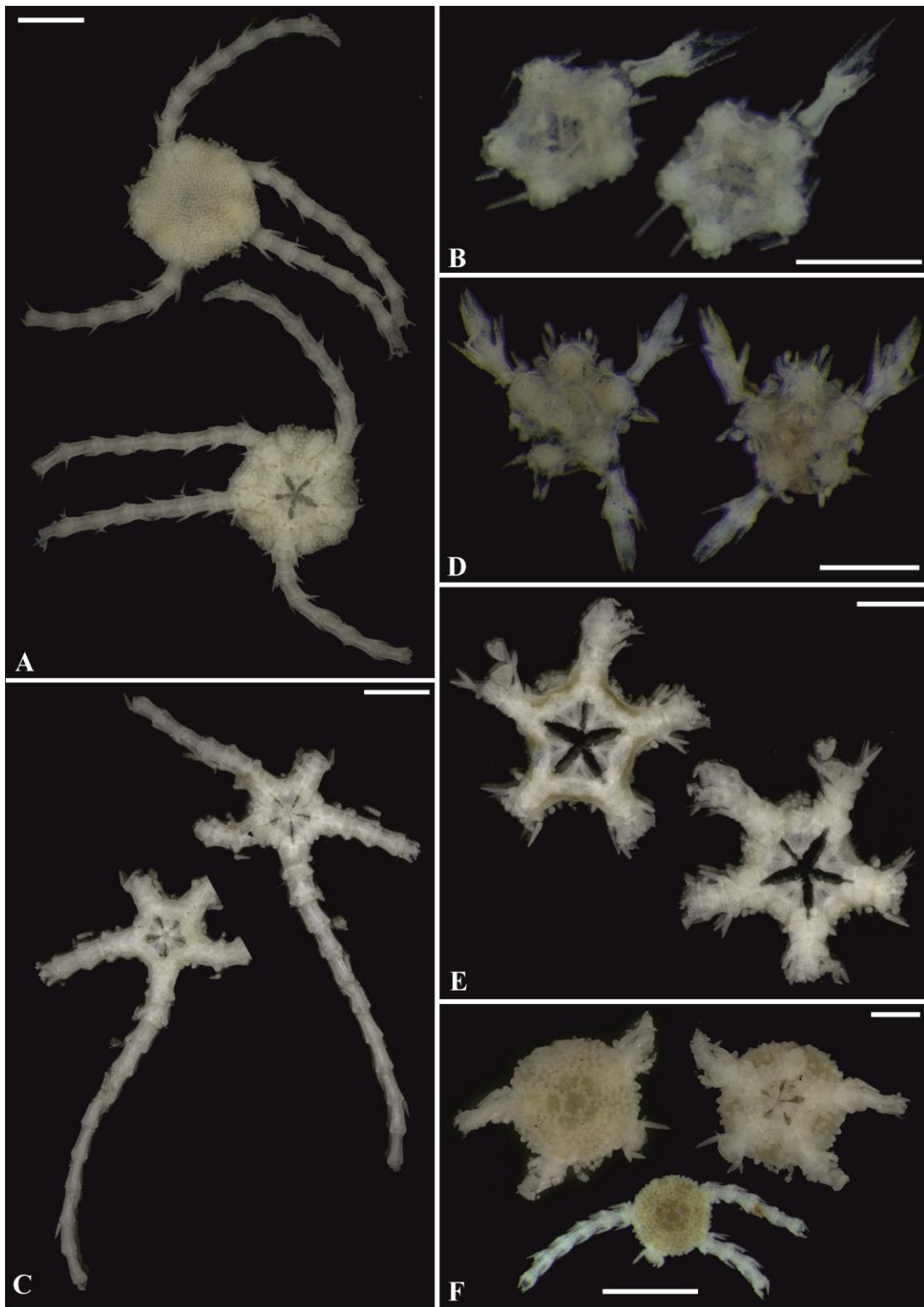


**Figure 8**

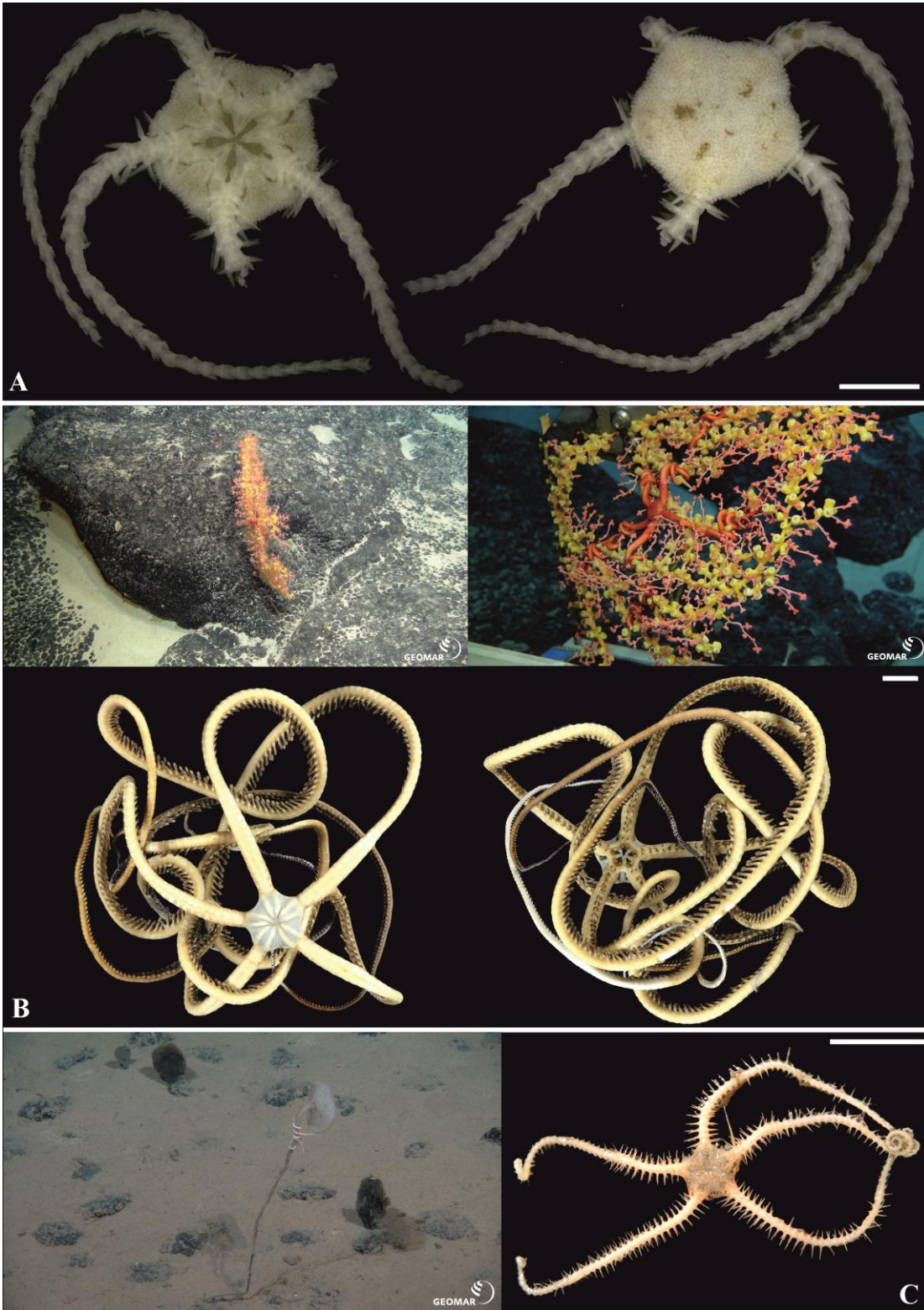


Figure 9

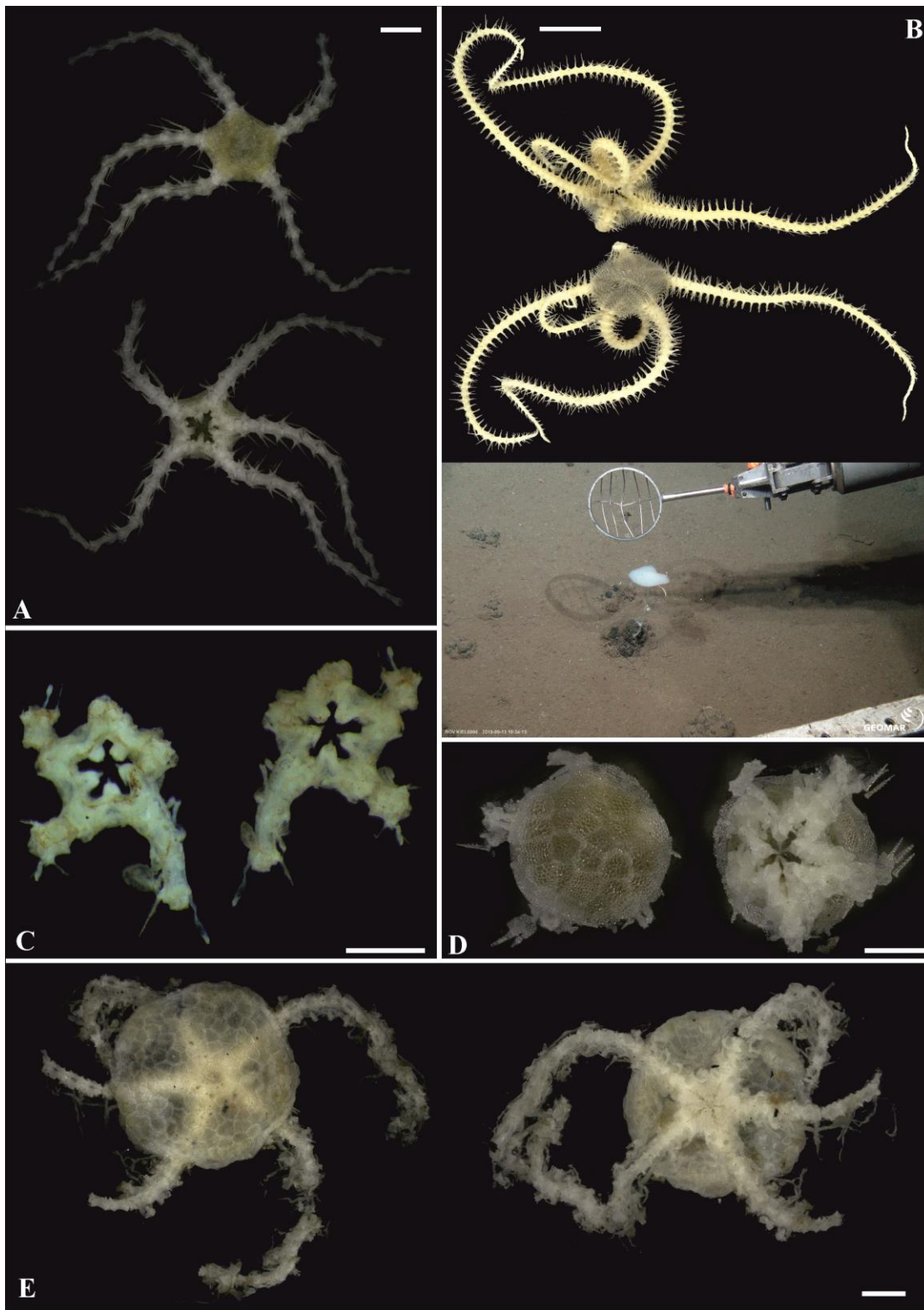
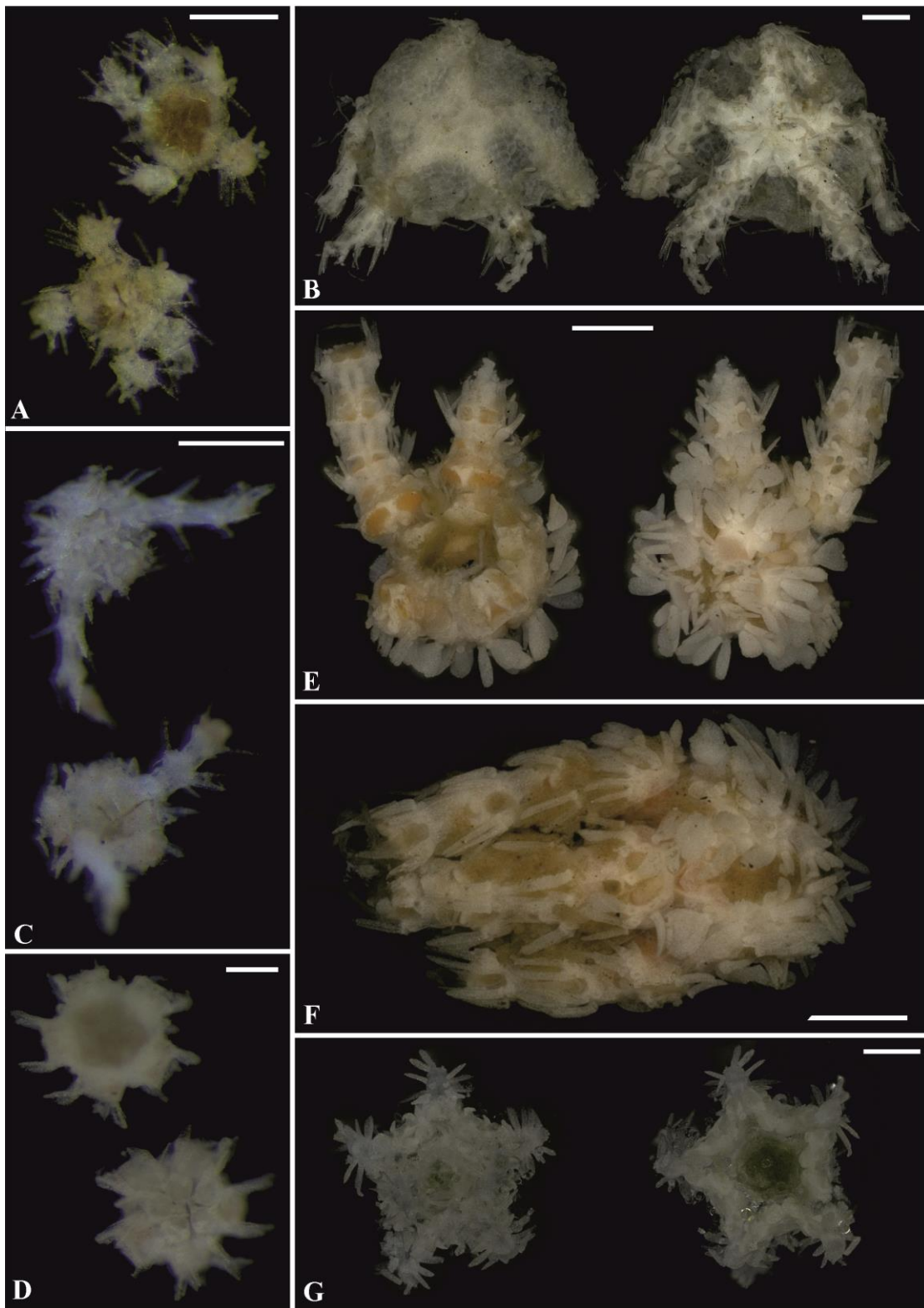
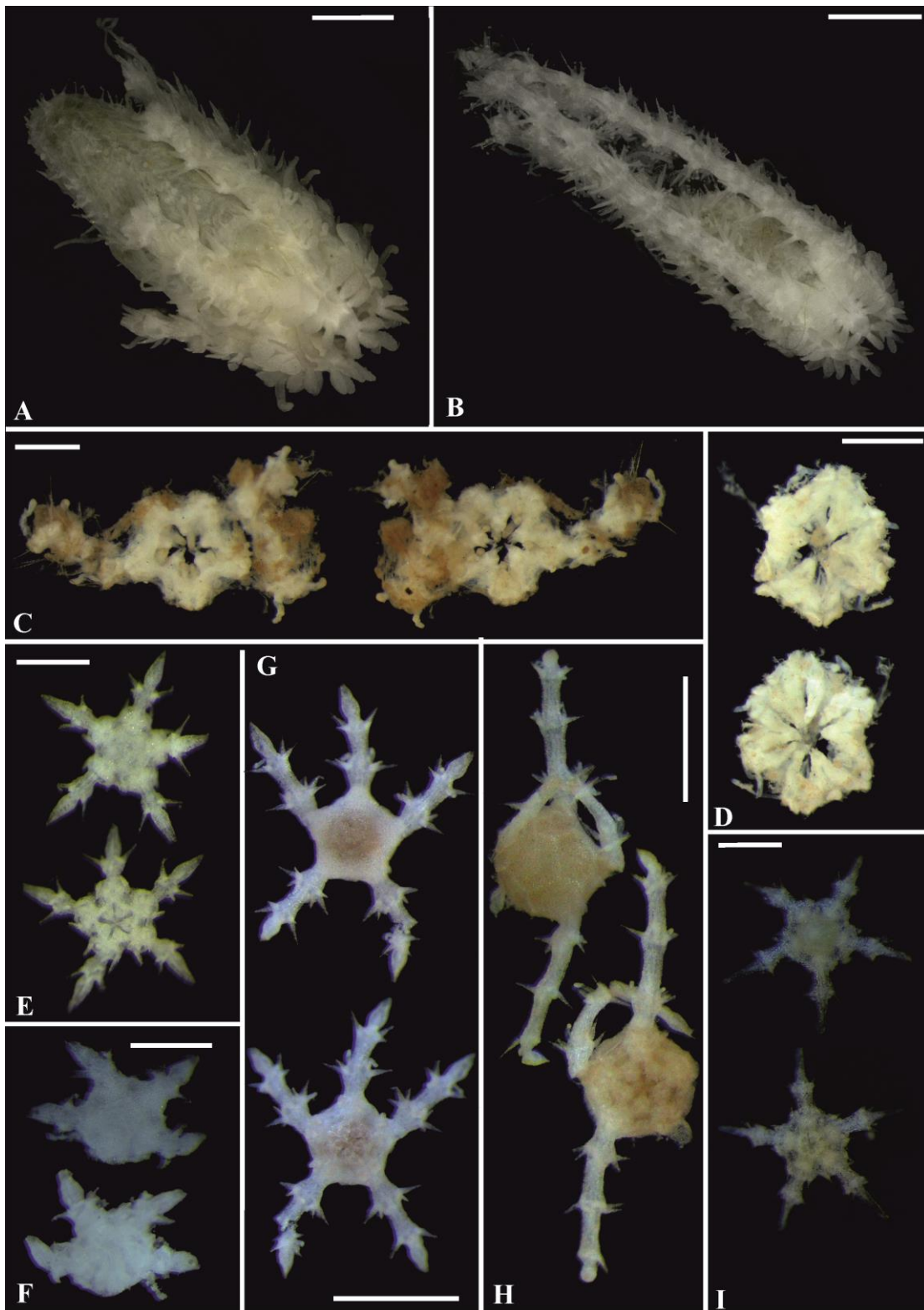


Figure 10



**Figure 11**



**Figure 12**

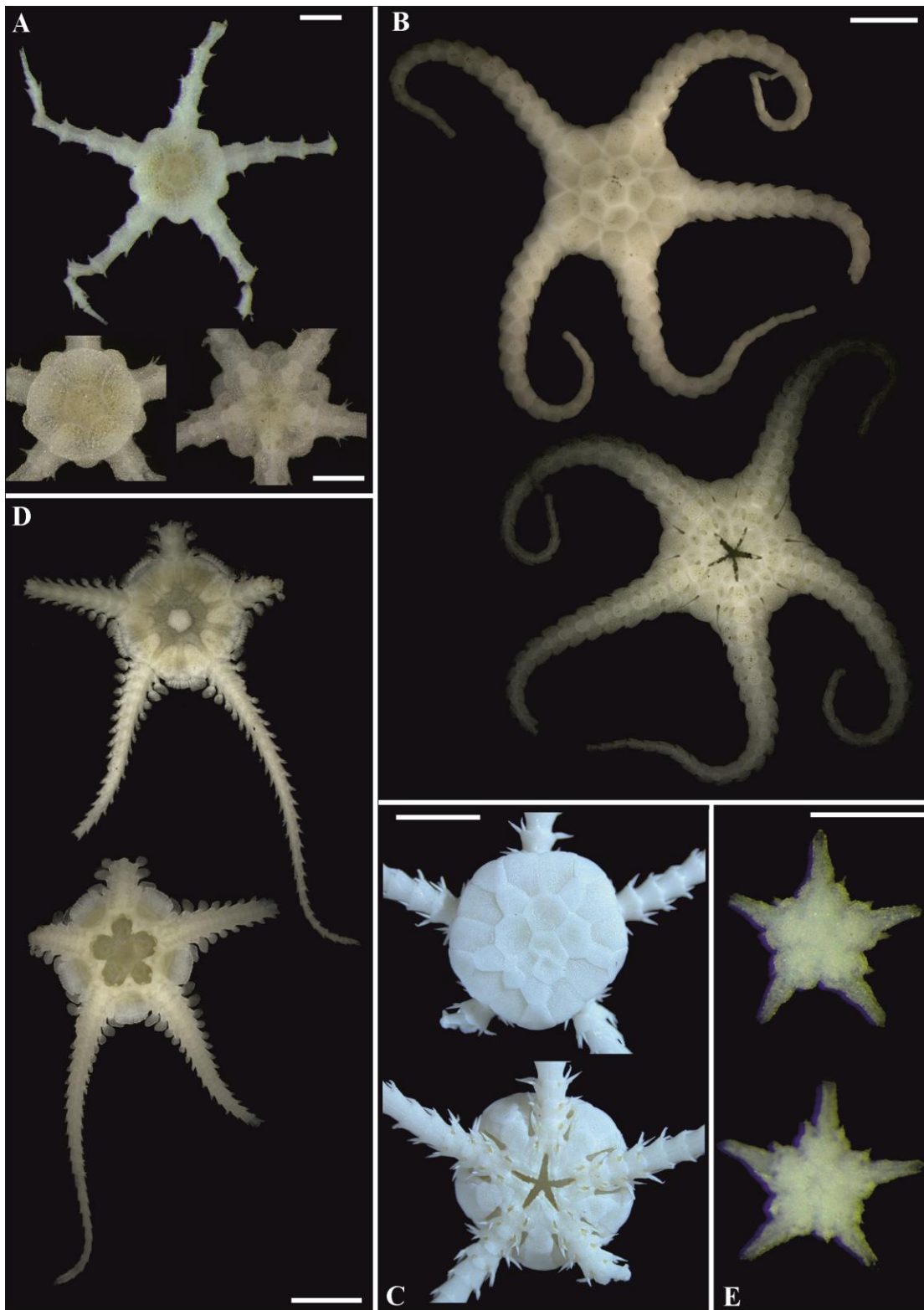


**Figure 13**

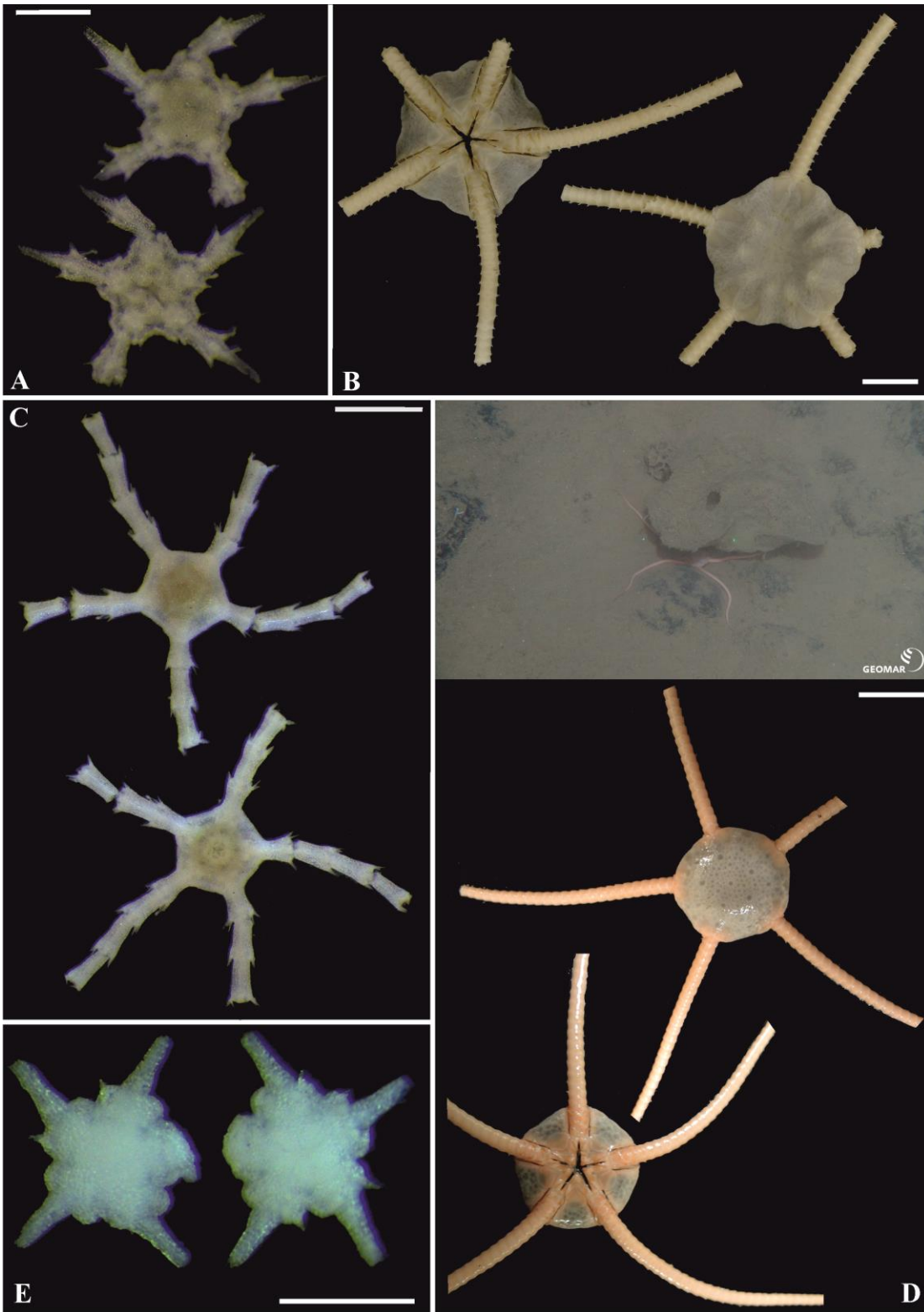
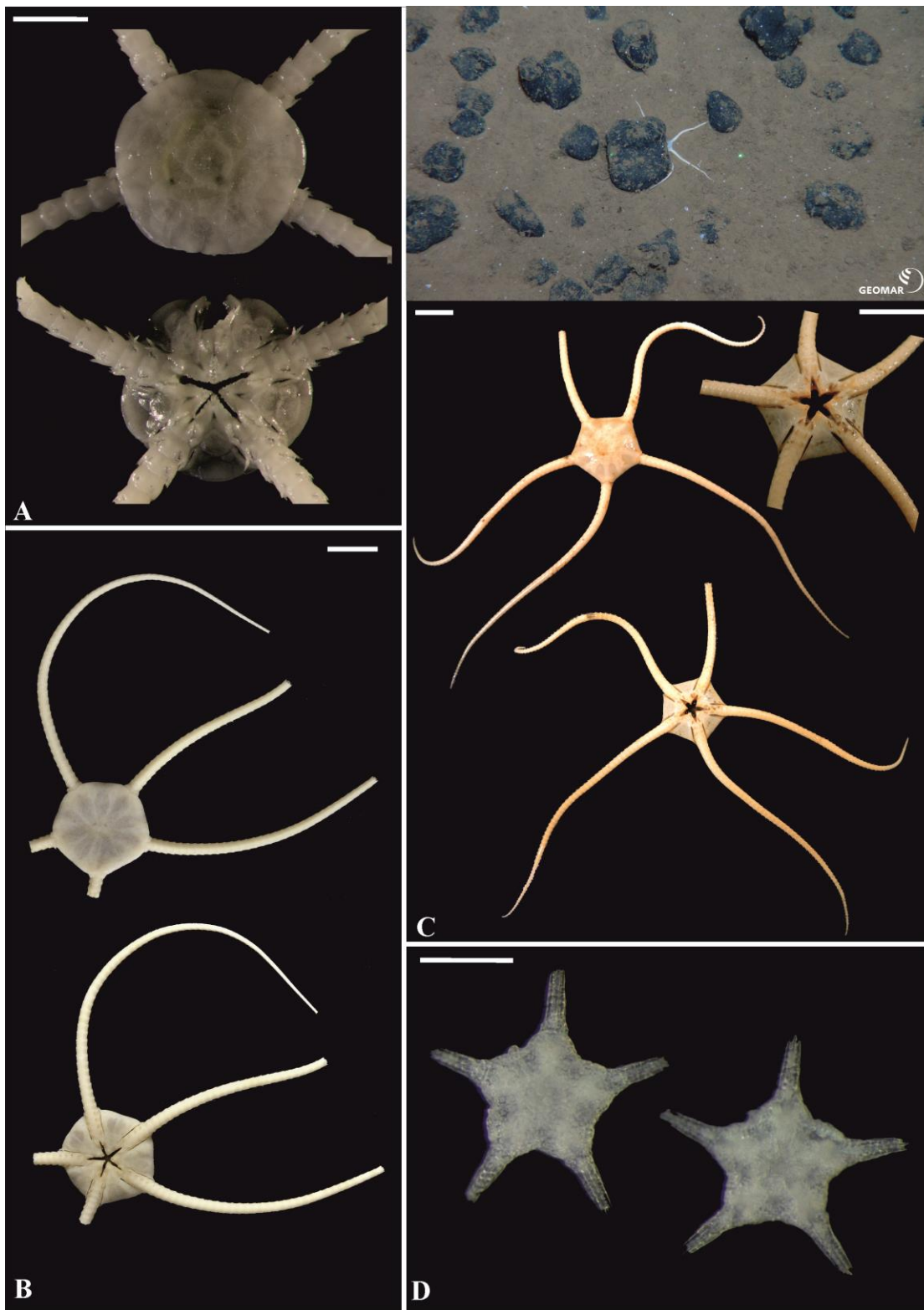


Figure 14



**Figure 15**

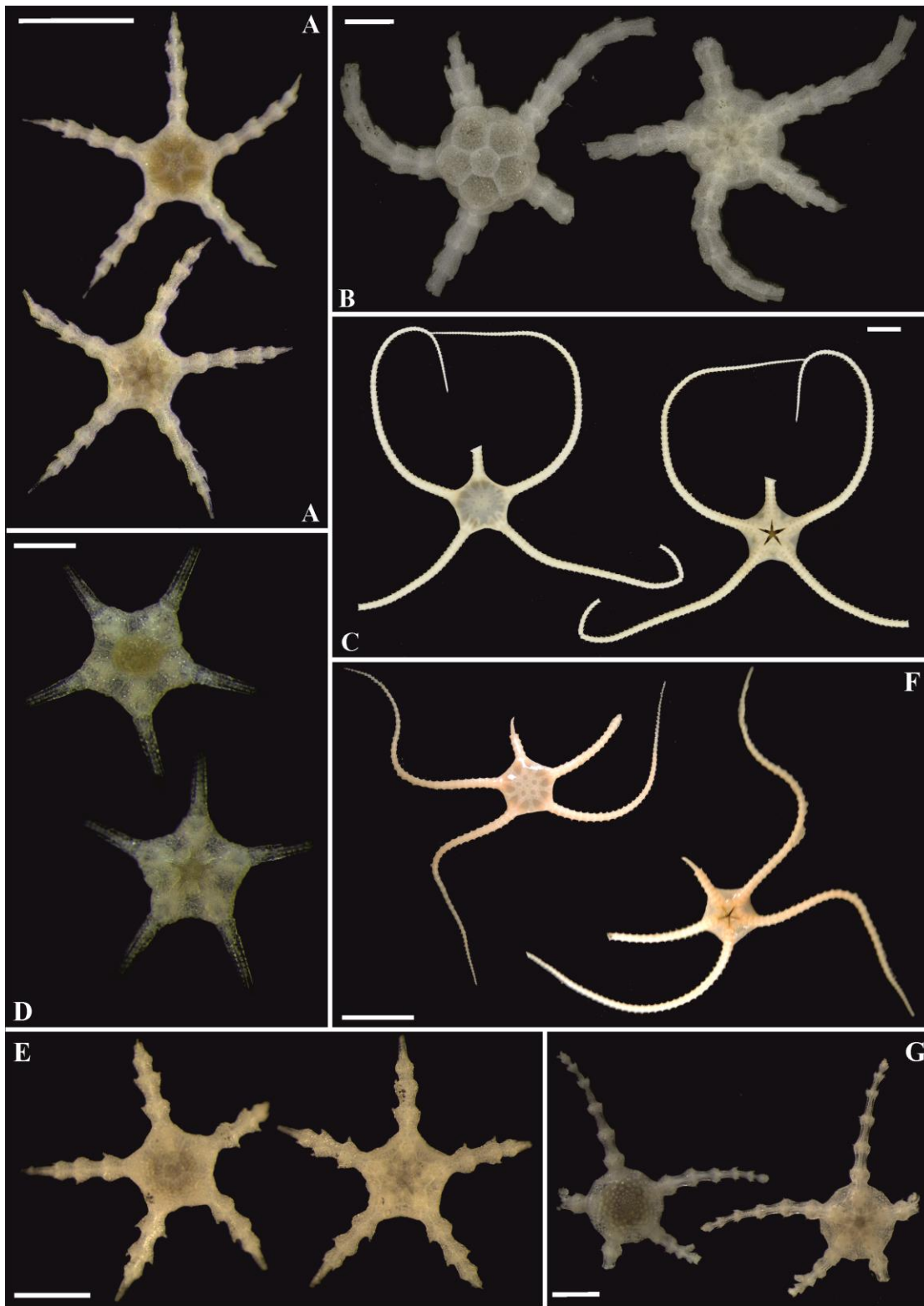


Figure 16

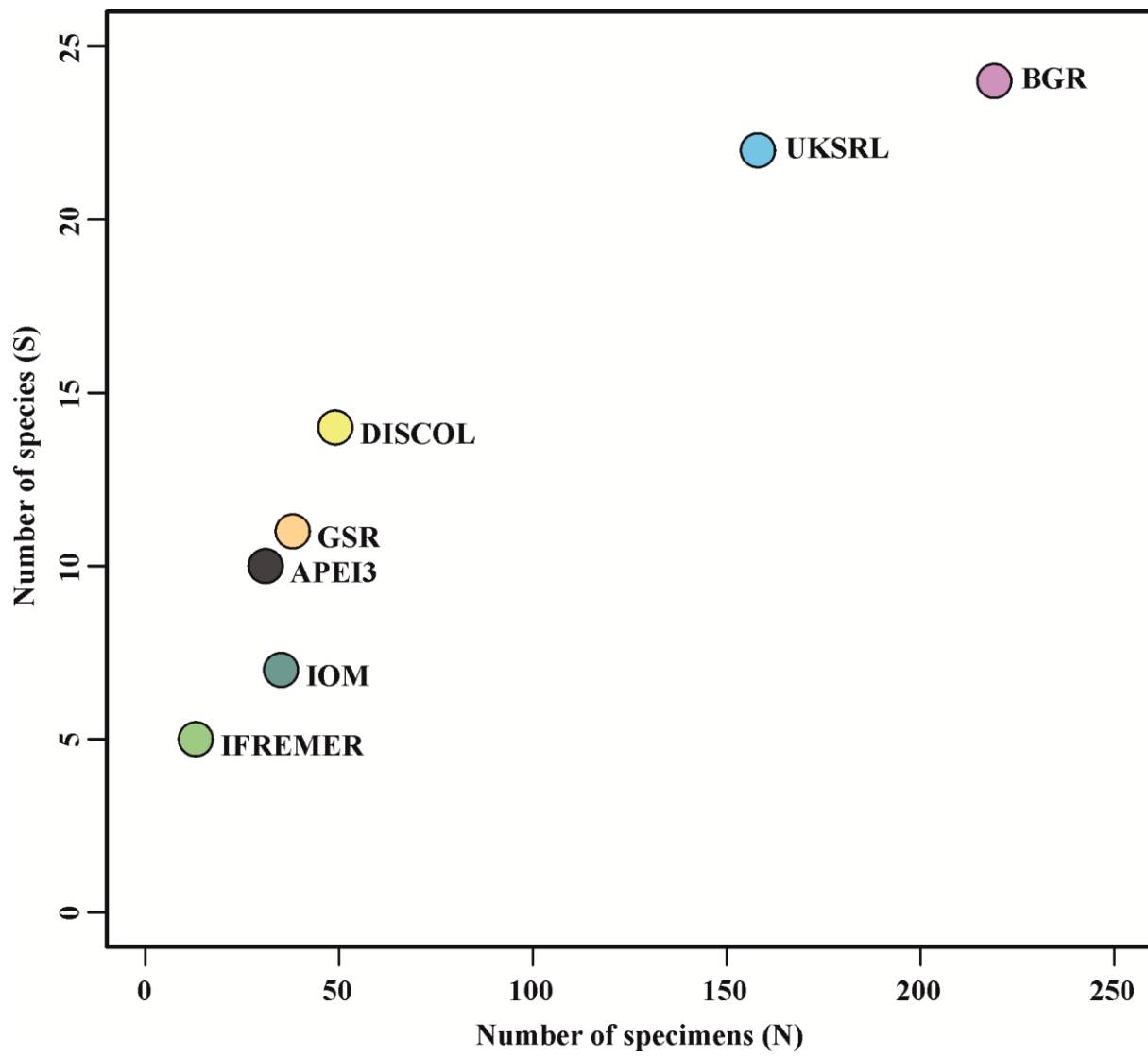


Figure 17

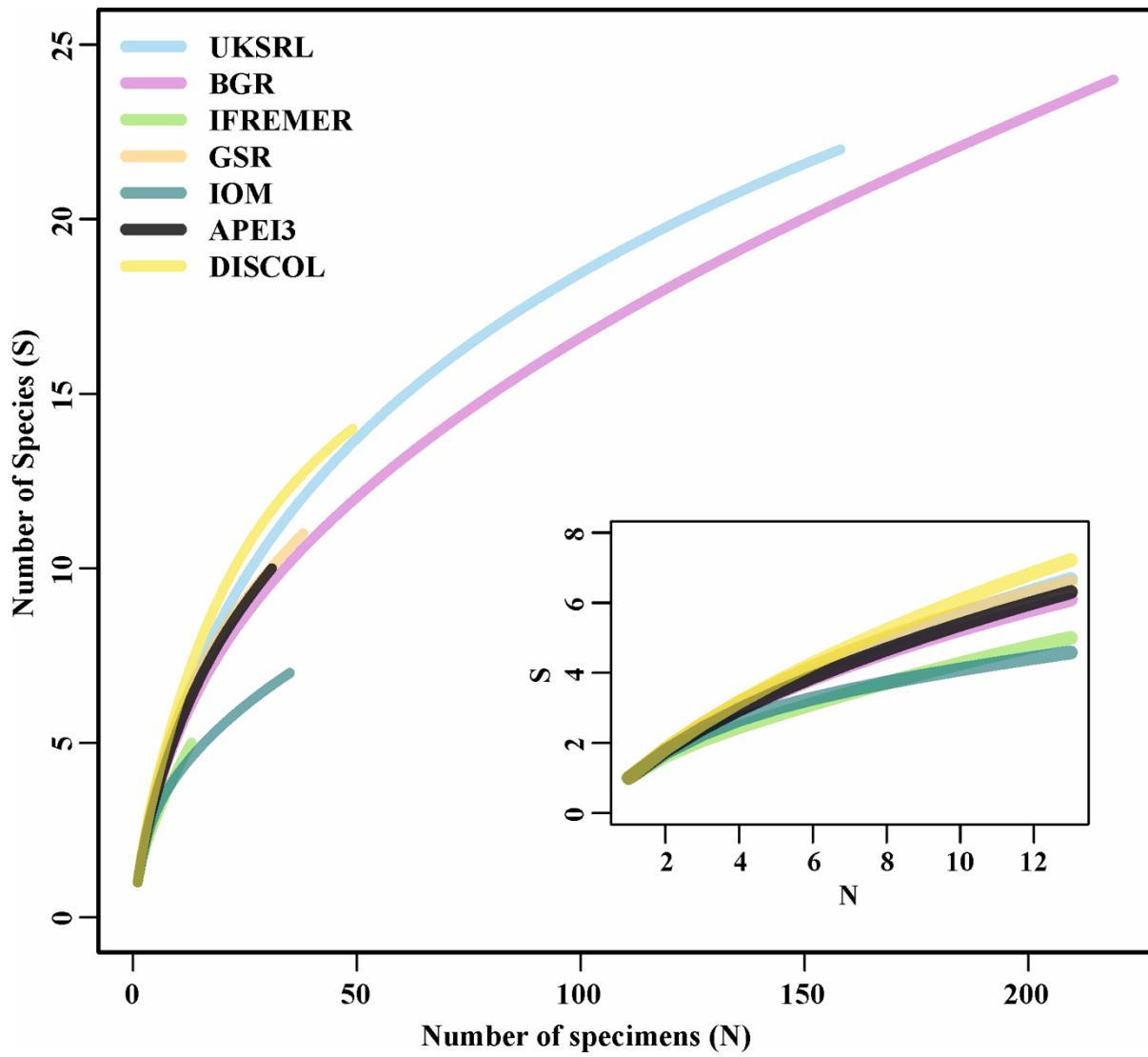


Figure 18

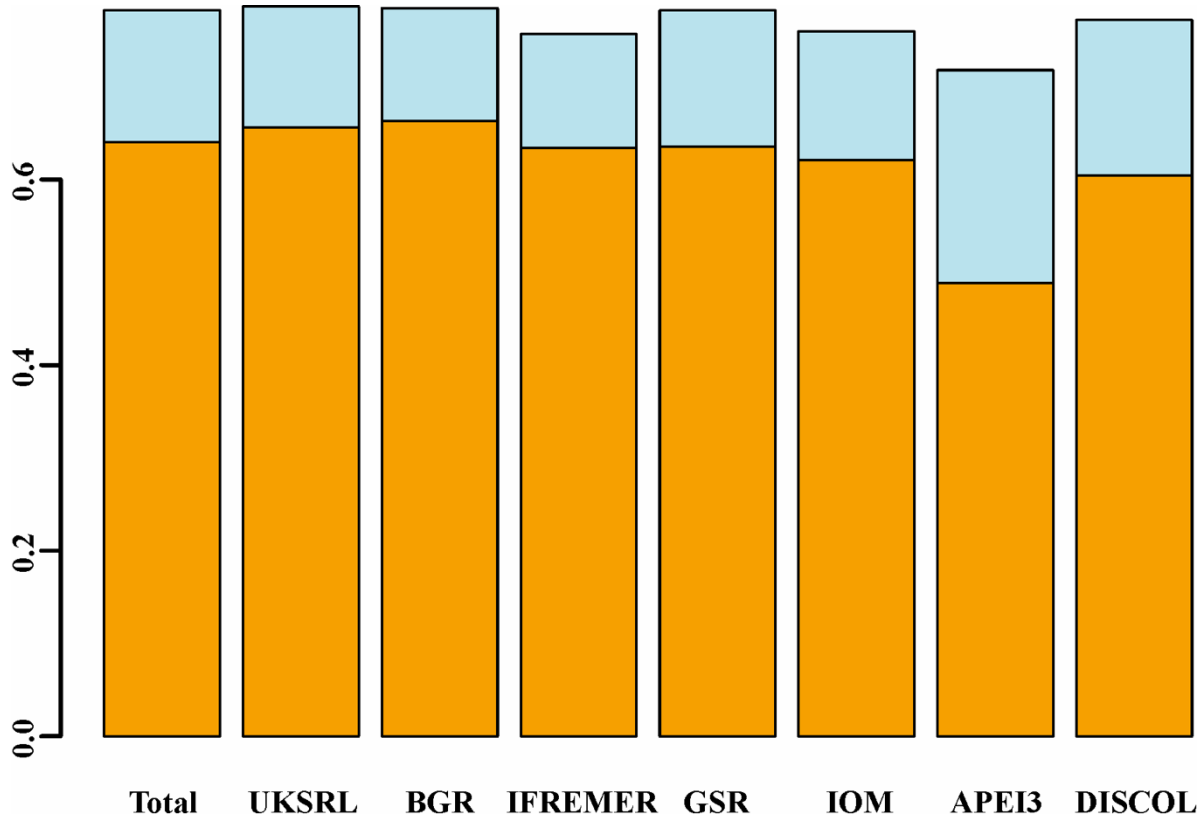


Figure 19

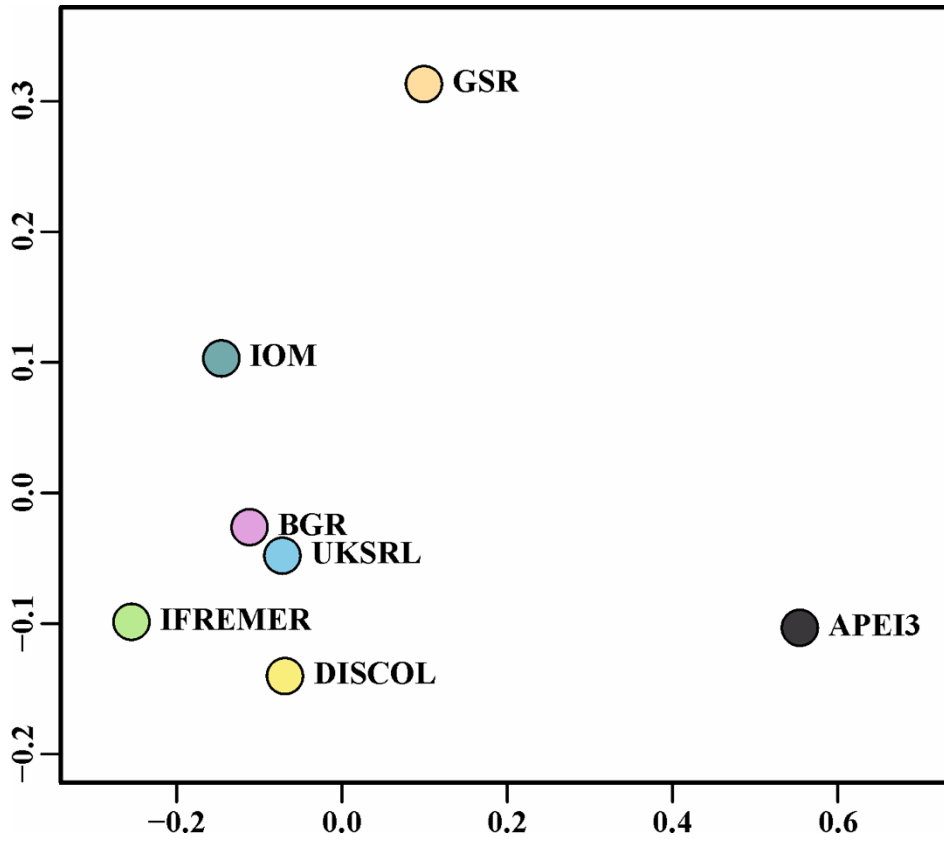


Figure 20

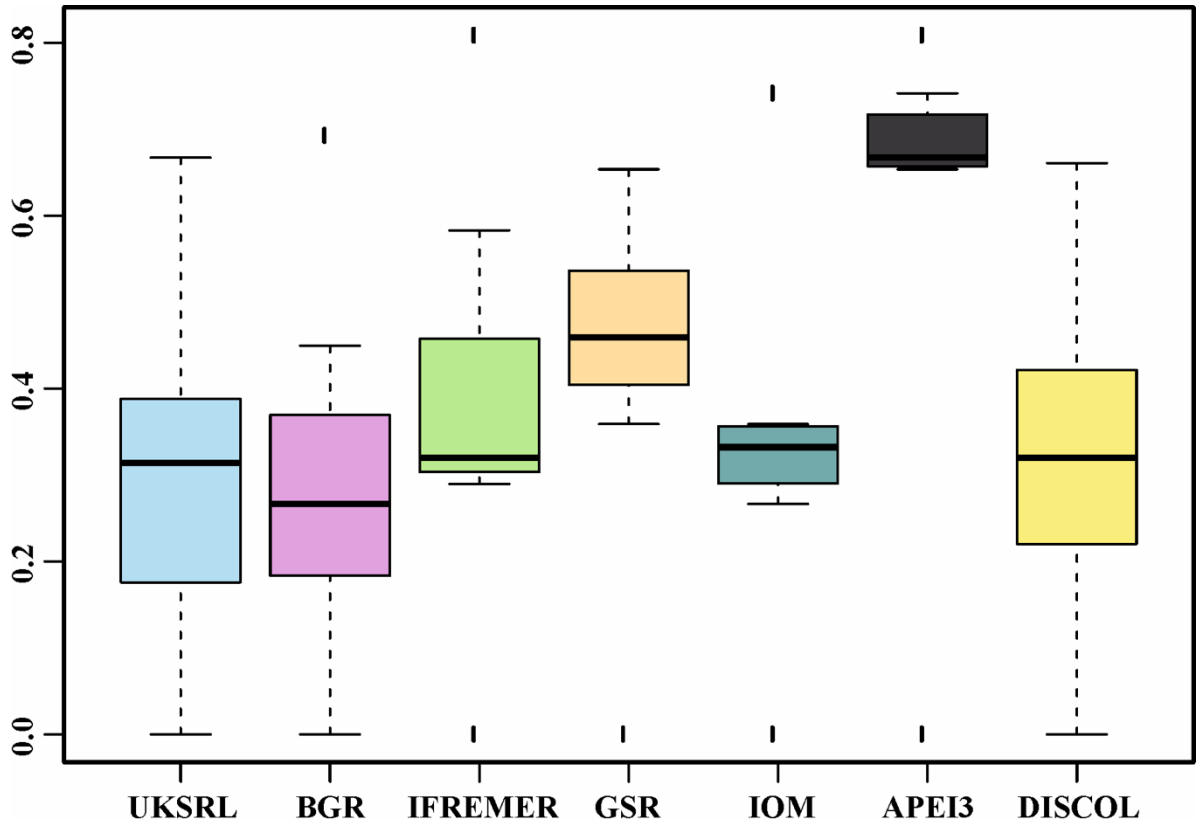


Figure 21

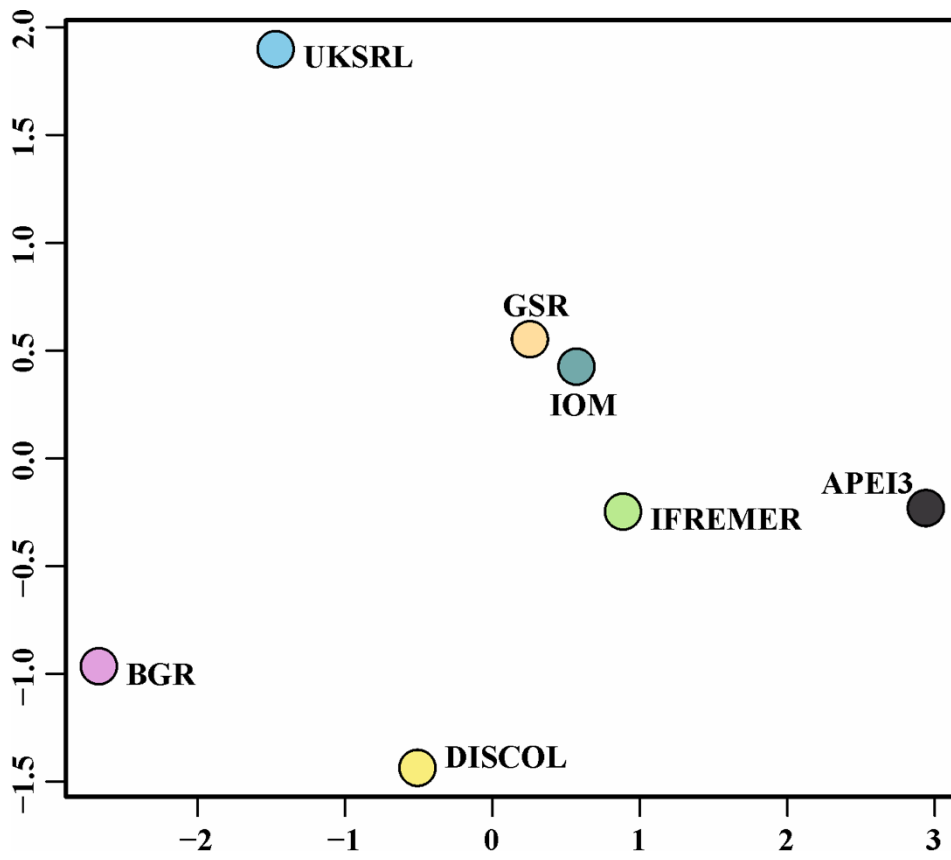


Figure 22

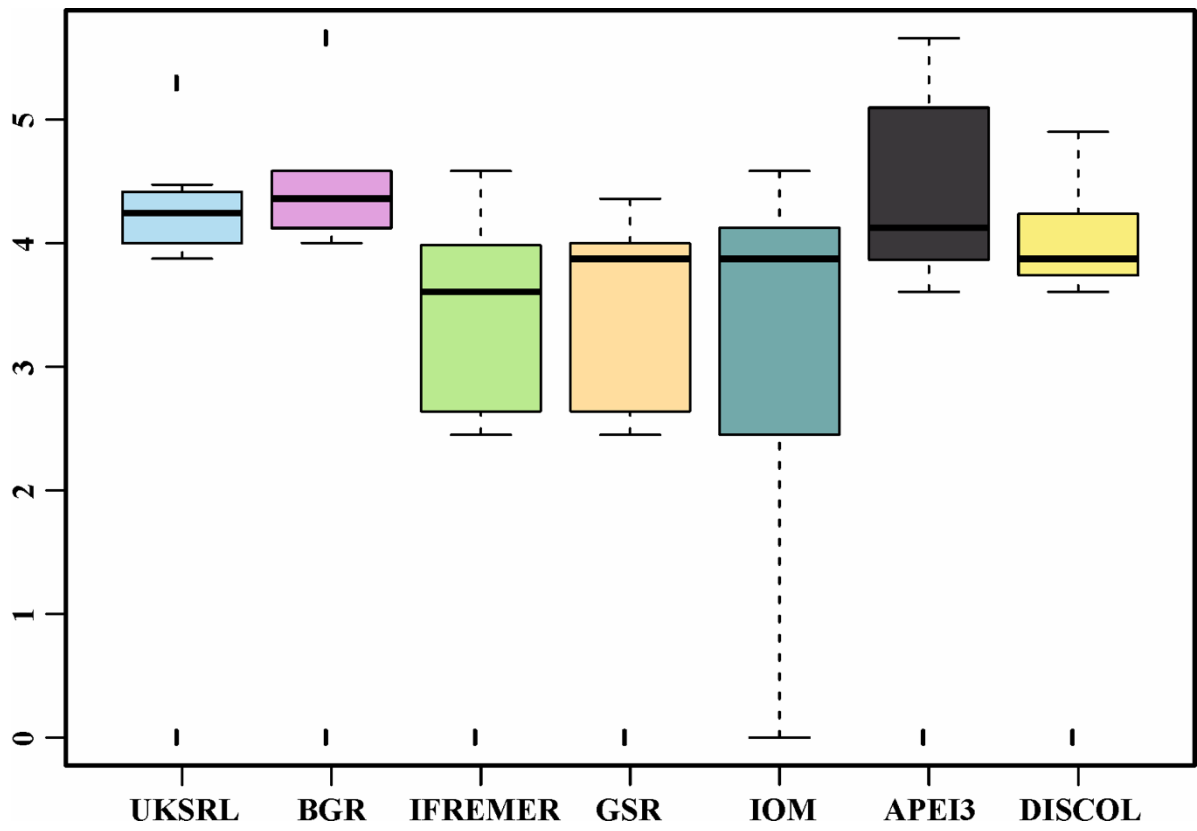


Figure 23